1-1-2005

Quantitative friction force microscopy for micro/nanoscale friction studies of joint replacement materials

Kanaga Karuppiah Kanaga Subramanian
Iowa State University

Quantitative friction force microscopy for micro/nanoscale friction studies of joint replacement materials

by

Kanaga Karuppiah Kanaga Subramanian

A thesis submitted to the graduate faculty

in partial fulfillment of the requirements for the degree of

MASTER OF SCIENCE

Major: Mechanical Engineering

Program of Study Committee:
Sriram Sundararajan, Major Professor
Pranav Shrotriya
Balaji Narasimhan

Iowa State University

Ames, Iowa

2005

Graduate College
Iowa State University

This is to certify that the master's thesis of

Kanaga Karuppiah Kanaga Subramanian

has met the thesis requirements of Iowa State University

Signatures have been redacted for privacy

TABLE OF CONTENTS

CHAPTER 1. Introduction

1.1 Micro/nanotribology and its significance

Tribology is the science and technology of two interacting surfaces in relative motion and of related subjects and practices. The popular equivalent is friction, wear and lubrication. Tribology is crucial to modern systems that involve sliding and rolling surfaces. The purpose of research in tribology is understandably the minimization and elimination of losses resulting from friction and wear at all levels of technology where the rubbing of surfaces is involved.

The advent of new techniques to measure surface topography, adhesion, friction, wear, lubricant film thickness and mechanical properties, all on a micro- to nanometer scale has led to the development of a new field referred to as microtribology, nanotribology, molecular tribology or atomic-scale tribology [1]. This field is concerned with experimental and theoretical investigations of processes ranging from atomic and molecular scales to microscales, occurring during adhesion, friction, wear and thin-film lubrication at sliding surfaces. At the micro/nanoscale, the surface properties, rather than the bulk would influence the tribological phenomena. Micro/nanotribological studies can provide a fundamental understanding of interfacial phenomena on a small scale which can be used to 1) improve the design of micro- and nano-components that are used in magnetic storage systems, micro electro mechanical systems (MEMS) and other industrial applications where components are very light operate under lightly loaded conditions and 2) develop strategies to engineer ultra-

low friction and wear surfaces in macroscale systems, providing a bridge between science and engineering.

1.2 Laws of sliding friction

Friction is the resistance to motion that is experienced as one solid body moves tangentially over another with which it is in contact. Friction between two bodies in contact depends upon the surface and bulk properties of the bodies, presence or absence of intervening contaminants and fluids as well as operating conditions. Two basic laws of intrinsic friction, developed by Guillaume Amontons in 1699 and referred to as Amonton's Laws, are generally obeyed over a wide range of applications. The first law states that the friction force (F) between two bodies is proportional to the normal load (N) between them, with the constant of proportionality μ, termed the coefficient of friction as given below

$$F = \mu N \qquad 1$$

The second law states that the friction force (or coefficient of friction) is independent of the apparent area of contact between two contacting bodies. Thus on the macroscale, two bodies of a particular material pair will exhibit the same coefficient of friction regardless of their physical shape and size. The coefficient of friction is the most widely used measure of the friction response of a material pair in engineering applications. A higher coefficient of friction corresponds to a higher friction response.

A more physical interpretation of friction forces was developed by Bowden and Tabor [2], who proposed that the total intrinsic frictional force (F_i) can be written as a sum of an adhesion process and a deformation process during sliding (assuming negligible interaction between the two processes) as follows:

$$F_i = F_a + F_d \qquad 2$$

where F_a is the force needed to shear adhered junctions and F_d is the force needed to supply the energy of deformation.

At interfaces of technological relevance, actual contact occurs at multiple asperity locations. When two nominally flat surfaces come into contact, the sum of the areas of all the contact locations constitutes the real (true) area of contact (A_r). For most of the materials under normal load, this is only fraction of the apparent (nominal) area of contact (shown in Figure 1.1). The proximity of the asperities results in adhesive contacts due to physical or chemical interactions. When these two surfaces move relative to each other, a lateral force is required to shear the adhesive bonds formed at the interface in the regions of real area of contact. Thus, the friction force would depend on the interfacial shear strength (τ_a) of the materials. From classical theory of adhesion to a very rough first approximation, the adhesive friction force (F_a) for a dry contact is defined as follows [2].

$$F_a = A_r \tau_a \qquad 3$$

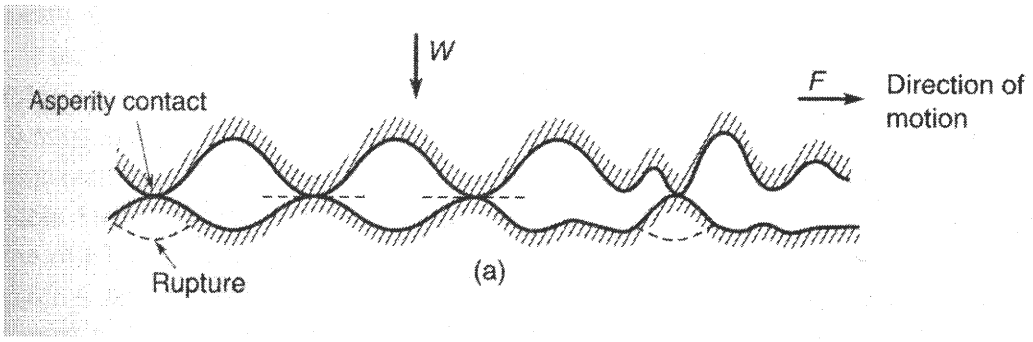

Figure 1.1 Schematic showing the real area of contact (A_r) which is only a fraction of the apparent area of contact. (Source: B. Bhushan, Principles and applications of Tribology)

Bowden and Tabor[2] recognized early on in their wide-ranging studies of friction that adhesion between materials can contribute significantly to friction, independent of contributions due to the ploughing of surface asperities. The deformation component arises as asperities of the harder material plough into the softer material and cause plastic deformation. This component of the friction is traditionally written in terms of asperity geometry and deformation groove geometry [3]. In general if the loads are low or if the contact area is large, the friction force is dominated by the adhesive component. Equation 3 gives us insight into controlling adhesive friction. The friction can be reduced by reducing the real area of contact or by reducing the interfacial shear strength. The latter approach is preferred since reducing the real area of contact beyond a certain value leads to onset of plastic deformation. Hence measuring and controlling the interfacial shear strength is of scientific and technological interest.

1.3 Atomic force microscopy

As discussed previously, contact occurs at multiple asperity contacts in interfaces of technological relevance. A sharp tip of a tip-based microscope sliding on a surface simulates one such (single asperity) contact, as shown in Figure 1.2. The atomic force microscope is such a tip-based microscope that provides the opportunity to measure tribological phenomena of interest at a single asperity scale.

Atomic force microscopy has emerged as one of the most versatile microscopic techniques in the past two decades. The introduction of the atomic force microscope (AFM) in 1985 [4] provided a method of measuring ultra-small forces between a probe tip and an

Figure 1.2 Schematic of a tip-based microscope (right) which simulates one of the multiple asperities shown on the left to enable single asperity scale measurements

engineering surface as well as provide surface topography information of surfaces with sub-nanometer spatial resolution. Since then, the AFM has been used and adapted for a variety of force and energy spectroscopy measurements on the micro/nanoscale including but not limited to adhesive and capillary forces, lateral (friction), electrostatic forces, magnetic forces, thermal gradients and chemical forces. , as well as for adhesion and electrostatic force measurements (an extensive list of references can be found in [5; 6]). As a result, the family of AFM-based techniques is now labeled scanning probe microscopy (SPM).

1.4 Lateral (friction) force microscopy

Subsequent modification of the AFM by Mate et al [7] led to the development of the lateral force or friction force microscope (LFM or FFM) in 1987, designed for atomic to micrometer scale studies of friction. Lateral Force Microscopy (LFM) is a scanning probe microscopy (SPM) technique that identifies and maps relative differences in surface frictional characteristics. LFM is used to provide a model asperity contact with a solid or lubricated surface and AFM-based experiments can reveal much about nanoscale nature of friction. Applied with contact mode atomic force microscopy (AFM), LFM is particularly useful for differentiating components of heterogeneous surfaces.

1.5 Overview of AFM and LFM operation

In standard contact mode atomic force microscopy (AFM), the probe is scanned over the surface (or the sample is scanned under the probe) in an x-y raster pattern. A laser beam is focused on the cantilever and reflects onto a segmented photodiode detector to monitor the deflection of the cantilever during raster-scanning. This is shown in Figure 1.3 (a). A feedback loop maintains a constant force on the sample by adjusting the height of the cantilever to compensate for topographical features of the surface resulting in a three-dimensional map of the sample. In LFM, the probe is scanned perpendicular to its length. Friction between the probe and surface will cause the cantilever to twist. The torsion, or twisting, of the cantilever will increase or decrease depending on the frictional characteristics of the surface (greater torsion results from increased friction). For LFM, as the probe is scanned sidewise, the friction signal is calculated as (A + C) - (B + D). For contact mode, the deflection signal is calculated as laser spot intensity for quadrants (A + B) - (C +D). Since the laser detector has four quadrants (Figure 1.3 b), it can simultaneously measure and record topographic data and lateral force data. Both of these data sets may be viewed simultaneously in real time, and stored and processed independently.

LFM is extremely useful for identifying surface compositional differences where the materials have differing frictional characteristics. It should be noted, however, that sharp changes in topography can cause transitions in lateral forces that are not related to the intrinsic friction response. Several studies have clearly established correlations between changes in local slope and lateral forces [8-10] and outlined methodologies to identify and minimize these topography-based artifacts. Contamination on the sample surface can also cause transitions in the friction response.

Figure 1.4 (a) shows the topography of octadecanethiol monolayer dots on a silicon substrate and (b) shows the corresponding friction image where the octadecanethiol dots show lower friction compared to the silicon substrate.

1.6 Quantitative friction force microscopy

The friction response measured in the microscope, as described in the previous section, is in terms of the voltage output of the lateral deflection signal, which in turn is a measure of the amount of torsion the cantilever undergoes. The measured signal is sufficient for studies that seek to identify regions of varying friction on surface. However studies seeking to quantify the friction force between the probe and the sample require the use of a calibration process that converts the measured signal to units of force. This calibration process is not a trivial task. Furthermore, a careful determination of the cantilever spring constants and the probe radius is also required.

Microfabricated cantilevers of various material, force constant, shape and size are commercially available today. The popular ones are the rectangular silicon and v-shaped silicon nitride cantilevers shown in Figure 1.5 (a) and (b) respectively. Calculation of the cantilever's force constant is a difficult task as it depends on the cantilever and tip dimensions. One can cannot easily measure the lever thickness and tip height even with a good scanning electron microscope. Any deviations in the calculation of thickness of the cantilever could result in gross error in the calculation of the force constant. Since the

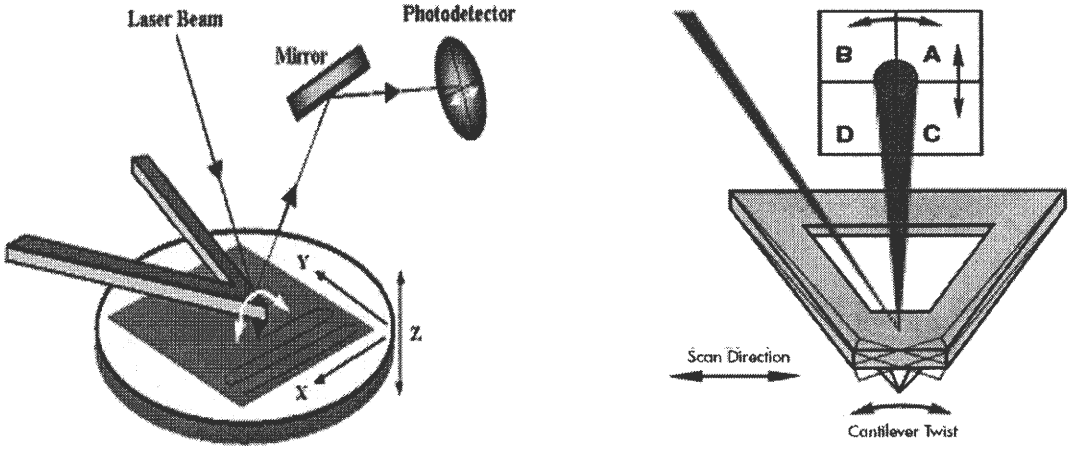

Figure 1.3 (a) Schematic of an AFM setup. Laser beam is impinged on the back of the cantilever which is reflected onto a four quadrant photodetector. (b) Schematic of a four quadrant photodetector – for topography (A+B)-(C+D) and for friction (A+C)-(B+D)

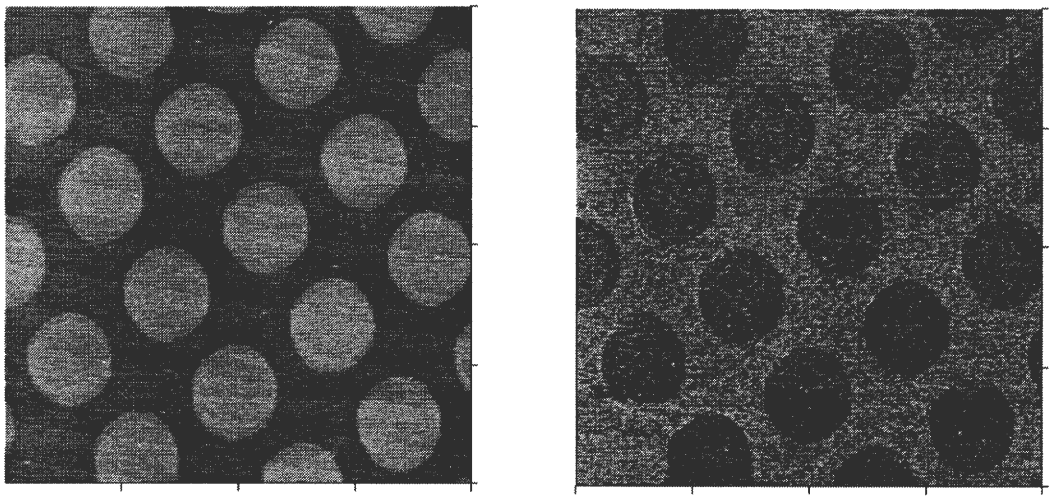

Figure 1.4 (a) 10 µm x 10 µm of height image of octadecanethiol (dots) deposited on silicon (b) Corresponding friction image shows lower friction on octadecanthiol dots compared to the silicon substrate.

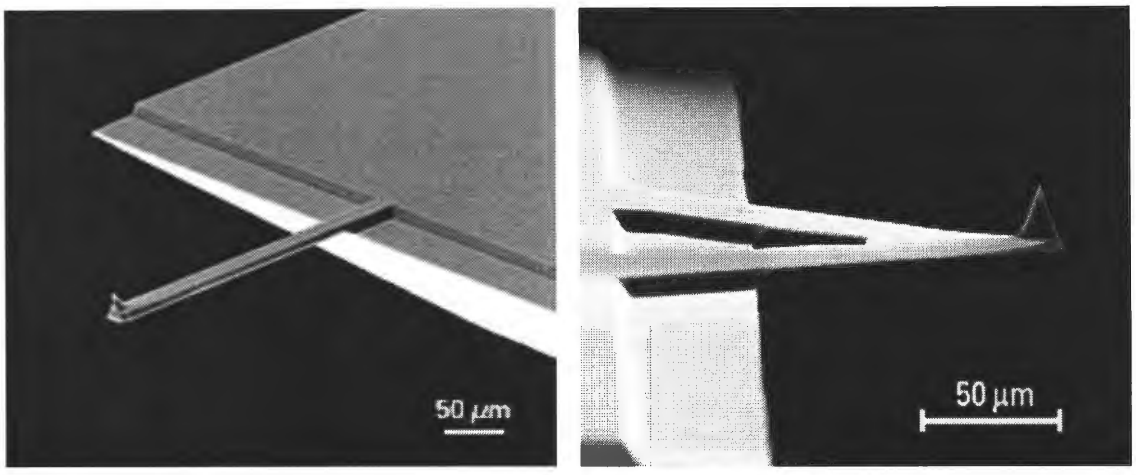

Figure 1.5 SEM image of a (a) rectangular silicon cantilever (left) and (b) v-shaped silicon nitride cantilever (right) (Source: www.spmtips.com)

cantilevers are produced by a chemical vapor deposition process, the mechanical properties of the cantilever can vary across the structure and moreover, some cantilevers are coated with a metal film to enhance reflectivity which could alter the cantilever's mechanical properties from the bulk. To overcome these issues in theoretical determination, spring constants are experimentally evaluated. While there are established methods for the fast and reliable measurement of normal spring constant [11-19], there is little research on lateral spring constant measurements [20-22].

Microfabrication techniques can produce sharp tips with tip radii ranging from a few nanometers to hundreds of nanometers. These tip radii can result in a contact area on the order of a few to a few thousand square nanometers. There is no way at present to directly measure the tip– surface contact area with a conventional AFM. However, the tip shape and size can be determined with some precision using commercially available calibration samples (Tipcheck from Aurora Nanodevices and TGT01 from MikroMasch USA, Portland, OR). Tipcheck has a Ti thin film coated on a Si surface and TGT01 has sharp spiked silicon

features. Both these samples exploit reverse imaging to provide a fast and simple way of assessing new tips i.e. these sharp features which when imaged using the AFM results in height maps that contain information regarding the tip shape (shown in Figure 1.6). Deconvolution of these images using blind reconstruction methods results in a fairly accurate estimate of the tip shape and radius [23; 24]. It is also important to note that the probe radius can change as a result of scanning on the surface [25], which can lead to a change in the friction response (Eq. 2). It is therefore of critical importance to monitor the probe shape during measurements.

The optical beam deflection sensor also poses a problem in quantitative friction measurements. Any measurement with an optical system would require the precise alignment

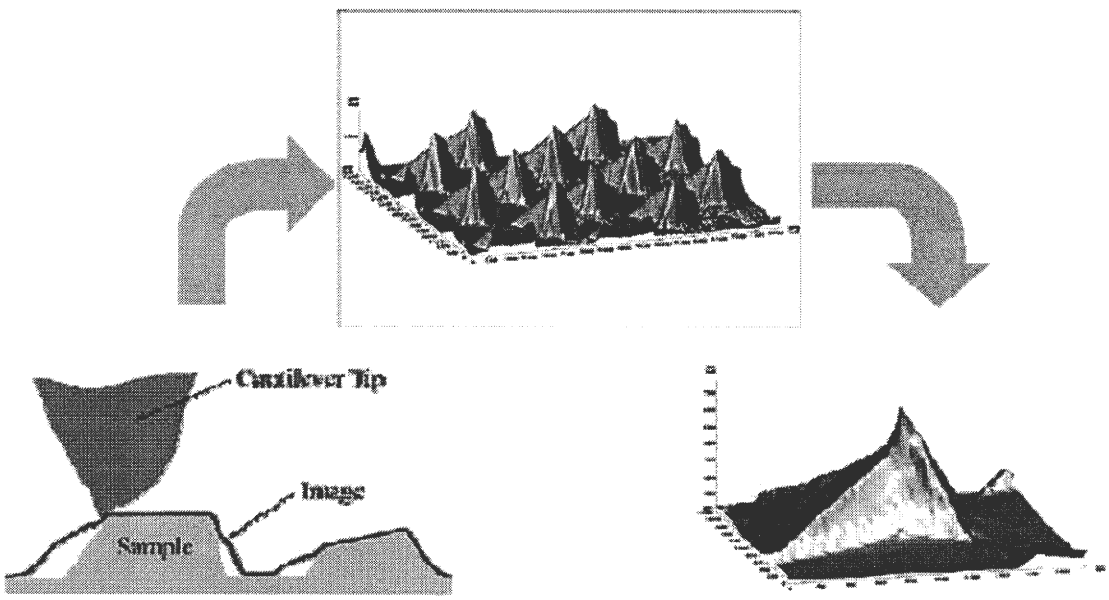

Figure 1.6 Schematic of reverse imaging concept used for monitoring tip shape and size. When an AFM tip scans across a spiked feature (Si, TGT01) sharper than the tip itself, height image of the tip itself is reproduced.

of the laser beam with respect to the cantilever. Also, the angular deflection of commercial cantilevers due to lateral forces is one to two orders of magnitude smaller than for normal forces, so small misalignment can cause significant errors in lateral force measurements due to cross-talk between normal and lateral deflections. Hence quantitative friction force measurements using an AFM are also dependent on the laser position and alignment on a given cantilever.

Several lateral calibration techniques exist to convert the measured lateral deflection signal in to force units [26-28]. However, no study has been performed to evaluate the validity of these techniques via comparison to a measured physical quantity such as interfacial shear strength.

1.7 Research objectives

The objectives of this research are:

1. To compare three widely used lateral force calibration methods for quantitative friction force microscopy, identify advantages and disadvantages associated with these techniques and identify a technique that is suited for standard commercially available Si_3N_4 cantilevers.
2. Perform quantitative friction force microscopy of a Si_3N_4 – Ultra-high molecular weight polyethylene (UHMWPE) interface and calculate the interfacial shear strength of the material pair. UHMWPE is a biomaterial used in artificial implants (total joint replacements) and whose friction characteristics affect the reliability and durability of the implant.

3. Investigate the dependency of the friction behavior and interfacial shear strength of UHMWPE on the exposure (soaking) time in bovine serum. The serum simulates synovial fluid, which acts as a boundary lubricant in human joints.

1.8 Thesis organization

In Chapter 2, an extensive literature survey of normal and lateral force calibration for AFM cantilevers is provided. Following the literature survey, three lateral calibration methods are described.

In chapter 3, results obtained from the three methods of calibration (described in chapter 2) on a common sample (silicon) are compared (research objective 1). Using the calibration methods, friction behavior of a Si_3N_4 – UHMWPE interface is quantified and the interfacial shear strength was calculated and compared to macroscale measurements from literature (research objective 2). The discrepancies in the shear strength calculations from the three methods were analyzed.

In Chapter 4, investigations into the effect of soaking time in bovine serum and concentration of bovine serum on the friction behavior of the Si_3N_4 – UHMWPE interface (research objective 3) are described. Quantitative AFM friction measurements, fluorescence measurements and contact angle measurements are shown for various UHMWPE samples soaked in bovine serum for specific time intervals. The changes in friction and shear strength of the interface are correlated to protein adsorption on the polymeric surfaces.

In chapter 5, the results of the research work are summarized and directions of future research are discussed.

CHAPTER 2. Overview of calibration methods in friction force microscopy

2.1 Introduction

Quantitative friction force measurements using an atomic force microscope (AFM) requires accurate determination of the cantilever spring constants as well as determination of a sensitivity factor that converts the measured lateral force response into force units. This chapter provides an overview of the various methods currently available to obtain these parameters.

2.2 Determination of spring constants

With the optical deflection technique used in an AFM, it became evident that for quantitative measurements of friction using AFM, the normal spring constant and lateral spring constant of the cantilever was required to be known accurately *a priori*. Two spring constants of the cantilever are of interest for friction measurements. The normal spring constant must be accurately determined in order to obtain correct values of applied normal load. Researchers started to tackle this issue in two ways – theoretical calculation and experimental determination. In the former method, one had to know the plane dimensions and mechanical properties of the cantilever very accurately, which as was described in the first chapter, are difficult to do. Slight deviations in these parameters (especially the thickness, which has a cubic power dependency) will lead to gross error in the quantization of the force (spring) constant. In the latter method, minimal parameters regarding the dimensions and mechanical properties of the cantilever were required. Consequently, these

methods are faster and more reliable. A review of some of the established methods is provided below

2.3 Determination of normal spring constant

V-shaped silicon nitride cantilevers have been the most used and popular probe for contact mode AFM imaging. Several researchers have come up with ways to calibrate the normal force constant or the spring constant of V-shaped AFM cantilevers. Two of the earliest and popular methods of calibration are by Cleveland et.al. [11] and Sader et.al. [13]. Cleveland et.al. [11] determined the spring constant of microfabricated cantilevers by measuring their resonant frequencies before and after adding small end masses. They also showed that the spring constant scales with the cube of the unloaded resonant frequency. Sader et.al. [13] obtained simple equations for the force constant of AFM cantilevers by parallel beam approximation of the v-shaped cantilevers. Sader et.al. [17] also came up with a method to determine the force constant of rectangular cantilevers which relies on measurement of the resonant frequency, quality factor and plane view dimensions of the cantilever. Sader et.al.[14] also found a fast and non-destructive method for v-shaped cantilevers which solely relies on the determination of the unloaded resonant frequency, knowledge of its density or mass and its dimensions. Senden et.al. [12] determined the spring constant by measuring the static deflection of a cantilever under the force of a known end-mass. Neumeister and Ducker [20] determined the force constant using theoretical analysis and finite element modeling which requires the plane dimensions of the lever. Holbery et.al. [18] have determined the force constant of cantilevers by using a commercial combination AFM and nanoindentation apparatus configured with a W-indenter tip. Gibson et.al. [19]

have presented a method of determining the force constant of AFM cantilevers that involves a simple expression that relates the spring constant of any two cantilevers on the same chip. This method requires the accurate determination of the force constant of one of the cantilevers on the chip by some other method. Torii et.al.[15] and Tortonese et.al. [16] used a reference cantilever of known spring constant to determine the force constant of test cantilevers.

2.4 Determination of lateral spring constant

While many methods to determine the normal force constant of AFM cantilevers exist, there have been relatively few studies to determine the lateral spring constant. Neumeister et.al. [20] determined the lateral force constant using theoretical analysis and finite element modeling which requires the plane dimensions of the lever. Green et.al. [22] have presented extensions of both the normal Cleveland method [11] and normal Sader method [17] to enable calibration of the torsional spring constants of AFM cantilevers. These extensions, referred to as torsional Cleveland and torsional Sader methods utilize a similar experimental setup to that of normal spring constant setup and hence, they give the advantage of simultaneous calculation of both normal and torsional spring constants of AFM cantilevers. Determination of the lateral spring constants did not eliminate the need to determine a conversion factor or calibration factor to convert the measured lateral force response to force units. In fact, as will be discussed in the next section, the methods developed to provide this calibration factor did not require the lateral spring constant.

2.5 Calibration methods for lateral (friction) force

Although numerous friction force microscopy studies reporting quantitative friction values on the nanoscale exist, they often differ in the technique used for lateral (friction) force calibration. The most widely used methods for lateral calibration are by Ogletree et.al. [27], Ruan and Bhushan [26] and Cain et.al. [28]. These three methods are the main focus of the present research and are explained in detail in the next section. In addition to these methods, several researchers have developed techniques that are not widely used due to the need for additional special measurement systems or due to large variability in data obtained. Pietrement et.al. [21] have developed a calibration method for lateral contact stiffness using modulated lateral force microscopy and this method is based on the study of the lateral contact stiffness versus applied load and on the use of elasticity contact theories to determine by fit the calibration coefficient. Liu et.al. [29] monitored the torsion signal as a voltage on a four-sector photo-diode and converted the torsion signal to a lateral force using the optical geometry of the instrument, cantilever dimensions and material properties. Fujisawa et.al. [30] obtained a calibration factor for the lateral force response of the cantilever directly from the initial "stick" portion of the friction loop, similar to Cain's method. Lantz et.al. [31] used scanning electron microscopy (SEM) to image and determine the geometry of the tip and based on the measured structure, they used FE modeling to arrive at values for lateral contact stiffness of the tip. They analyzed the stiffness of the tip sample contact and found that for a sharp tip the contact stiffness can be comparable to the lateral stiffness of the cantilever and ignoring the contributions of either of these stiffnesses would result in gross error in the accurate determination of the calibration factor.

In the following sections, a brief overview of the lateral force calibration techniques developed by Ogletree et.al. [27], Ruan and Bhushan [26] and Cain et.al. [28] are presented.

2.6 Overview of Ogletree et.al.'s method

Ogletree et.al.'s method [27] is an in-situ method of lateral calibration wherein the lateral response of a cantilever is measured in terms of normal force signal on a sloped surface. When a cantilever is forced to move on a sloped surface, there is a known geometrical contribution to the lateral force which is the product of the applied load and tangent of the slope. Using this principle, an experimental calibration factor is calculated by sliding a tip across a surface of a known slope and measuring the lateral force signal as a function of applied load.

Ideally, this method can be used on any surface which is tilted with respect to the lateral scanning direction. But Ogletree et.al have pointed out that this is not the case in practical situations. If the surface is tilted manually, there is an uncertainty in the tilt angle. Also, since the microfabricated tip is very short, there is a very good possibility that the sides of the tip are in contact with the tilted surface too. In order to avoid these experimental difficulties, they suggested using faceted $SrTiO_3$ (305) surface. The $SrTiO_3$ (305) surface forms two ridges along the (101) and (103) planes upon annealing in oxygen. The two planes are tilted at 14° and 12.5° respectively. This forms a good sample surface for Ogletree et.al.'s calibration method. However, $SrTiO_3$ surfaces are difficult to realize. As an alternative, commercially available silicon ridged surfaces (for e.g. from MikroMasch USA, Portland,

Oregon) can be used for Ogletree method. These surfaces have two slopes which are tilted at equal angles of 55°.

The two forces applied by the tip on the surface, the vertical load (L) and the horizontal tractive force (T) is balanced by a reaction force from the surface acting on the tip. This force is divided into two components namely, friction component, f and normal component, N. When the tip is slid across the surface, these forces are at equilibrium. They can be written as – (with '+' denoting uphill and '-'denoting downhill)

$$N_{\pm} = L \cos\theta \pm T_{\pm} \sin\theta \qquad \mathbf{1}$$

$$f(N_{\pm}) = T_{\pm} \cos\theta \pm L \sin\theta \qquad \mathbf{2}$$

Experimentally, the voltage output from the lateral force transducer or the photodiode response in commercial AFMs, T_o where $\alpha\ T_o = T$ is measured. T_o is the force measured in volts. α gives the direct calibration factor for the lateral force response in Newtons per Volt.

In commercial AFMs, the frictional force is determined by taking half the difference between the left-to-right and right-to-left lateral deflection forces or in other words, the half-width of the friction loop W(L), where L is the normal load. But in Ogletree's method, since the surface is tilted, the effective load is direction-dependent. Also, the offset of the friction loop represented by $\Delta(L)$ is not zero and depends on load. The following schematic from their paper shown in Figure 2.1 explains the above discussion.

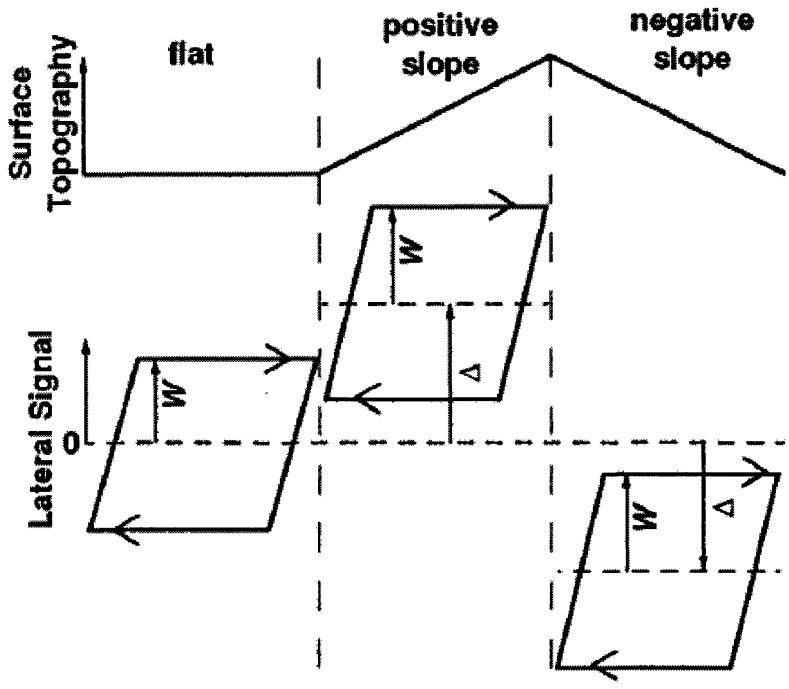

Fig. 2.1 Schematic of the change in friction loop width and offset when the tip slides on a flat surface, positive and negative sloped surfaces (Source: Ogletree et.al. [27])

For experimental purposes, they measured the lateral forces for a range of applied loads and used the slopes $\Delta' \equiv d\Delta/dL$ and $W' \equiv dW/dL$ in calculations, which are independent of L.

$$\alpha \Delta_0' = \Delta' = (1 + \mu^2) \sin\theta \cos\theta / \cos^2\theta - \mu^2 \sin^2\theta \qquad 3$$

and

$$\alpha W_0' = W' = \mu / \cos^2\theta - \mu^2 \sin^2\theta \qquad 4$$

Using these two equations, one can calculate the tip-surface friction coefficient and lateral force calibration constant. The ratio of these expressions gives μ.

$$\mu + 1/\mu = 2 \Delta_0'/ W_0' \sin 2\theta \qquad 5$$

Since μ and $1/\mu$ are equally good solutions which will give different values for α, two solutions μ can be obtained. The more reasonable one would be the value less than unity (which is a physically acceptable value for the coefficient of friction).

2.7 Overview of Ruan and Bhushan's method:

Briefly, in Ruan and Bhushan's method [26], the tip is first scanned across the surface in a direction parallel to the long axis of the cantilever over a range of normal loads in the elastic regime. The coefficient of friction (COF) is obtained from the slope of a plot of profile separation ('Trace-Retrace', TMR value at each scan location) as a function of average piezo center and probe/cantilever geometry.

In Ruan and Bhushan's method, when we scan in a direction parallel to the long axis of the cantilever, in addition to topographical imaging, it is also possible to measure friction force. If there were no friction force between the tip and the sample, the topographic feature would be the only feature to cause the cantilever to be deflected vertically. But, friction force exists on all contact surfaces where one object is moving relative to another. The friction force between the sample and the tip will also cause a cantilever deflection. It is assumed that the normal force between the sample and the tip is W_0 when the sample is stationary and the friction force between the tip and the sample is W_f. The direction of friction force is reversed as the scanning direction of the sample is reversed from positive to negative directions ($W_{f(y)} = -W_{f(-y)}$).

In contact mode, the vertical deflection is set at a constant level, and so is the total force applied to the cantilever. Since, the friction force is reversed on scanning in opposite

directions; the normal force will have to be adjusted accordingly so that the total force (normal force and friction force) will remain the same. By applying a total moment to the end of the cantilever and taking the attachment of the cantilever to the chip as the base point P (as shown in Figure 2.2), we can write the following relationships.

$$(W_0 - \Delta W_1) L + W_f l = (W_0 + \Delta W_2) L - W_f l, \qquad 6$$

Thus

$$W_f = (\Delta W_1 + \Delta W_2) L / (2 l), \qquad 7$$

where ΔW_1 and ΔW_2 are the absolute value of the changes of normal force when the sample is traveling in –y and y directions.

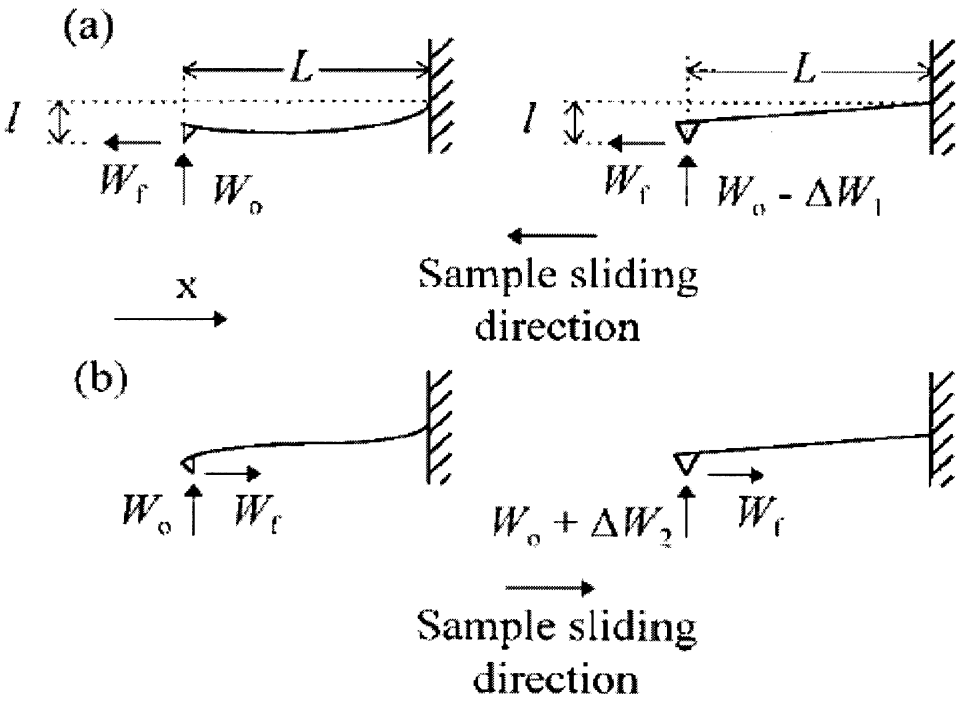

Fig. 2.2 Schematic showing the bending of the cantilever due to the frictional force when scanned in a direction parallel to the long axis of the cantilever (left). On the right are the adjusted normal force to keep the total force constant (Source: Cain et.al. [28])

L is the length of the cantilever and l is the vertical distance between the end of the tip and the base of the cantilever. The coefficient of friction (μ) is then given as:

$$\mu = W_f / W_0 = (\Delta W_1 + \Delta W_2) L / W_0 (2 l). \quad \textbf{8}$$

If the adhesive forces and the interatomic attractive forces are neglected, then the normal force W_0 is the equal to the initial cantilever deflection, H_0 multiplied by the spring constant of the cantilever. ($\Delta W_1 + \Delta W_2$) can be measured by multiplying the same spring constant by the height difference of the PZT between the two traveling directions (y and –y directions) of the sample. So, the above equation is rewritten as

$$\mu = W_f / W_0 = (\Delta H_1 + \Delta H_2) L / H_0 (2 l) \quad \textbf{9}$$

A modified approach of the above is to take the measurements at different normal loads and use $\Delta (H_0)$ and $\Delta (\Delta H_1 + \Delta H_2)$.

Once the coefficient of friction is determined, contact mode scans perpendicular to the cantilever axis are performed, again in the elastic contact regime for various loads. The friction force signals for a number of normal loads during trace and retrace scans are obtained. A 'true' friction signal is obtained by {FFMtrace – FFMretrace}/2 in order to eliminate errors due to misalignment between the vertical deflection line of the cantilever and the vertical line of the photodetector. By equating the slope of this plot (Volts/Newton) to the value of coefficient of friction, the torsional conversion factor for the FFM signal in Newtons/Volt can be obtained for the given tip/cantilever.

2.8 Overview of Cain et.al.'s method

Cain et.al. [28] have developed a technique to calibrate the lateral deflection signal for a colloidal probe and they extended it to standard AFM tips also. According to authors, previous calibration techniques have ignored or avoided the lateral stiffness of the tip-sample contact as they have pointed out that the lateral tip-contact stiffness and lateral cantilever stiffness are similar in magnitude for most practical friction experiments. Hence, the effect of the lateral contact stiffness cannot be neglected. Carpick et.al. [32] used the analogy of two springs in series to model the above behavior. Using Hertzian contact theory, they showed that in the case of a microfabricated tip contacting a mica surface, the contact stiffness in the normal direction is far greater than the cantilever stiffness. Whereas, in the lateral direction the contact stiffness and cantilever stiffness are similar in magnitude. Cain et.al.[28] follow in lines of Carpick et.al.[32] in using two springs in series to analyze the lateral deflection of the cantilever.

Experimentally, the friction measurements are recorded in friction loops. The photodiode response to torsion in the cantilever, V_{LFM}, is plotted against lateral piezo displacement. In the initial portion of the trace, the surfaces "stick" until the static friction is overcome. If the contact were infinitely stiff, all the deflections would occur in the cantilever. So, the lateral scanner movement would occur only because of the twisting of the cantilever. Hence, the slope S of the stick portion can directly be taken as the lateral calibration factor to scale the lateral photodiode output. But, in practical systems, this is not the case. The lateral contact stiffness has a finite value which influences the slope.

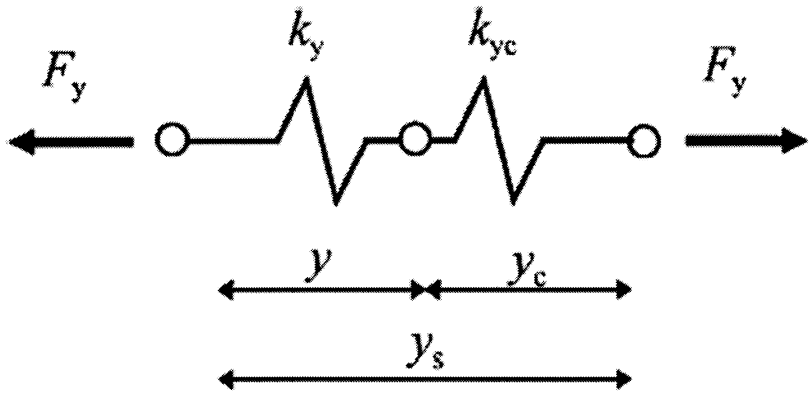

Fig. 2.3 Interpretation of AFM lateral deflection signal as two springs in series. The two springs represented by the lateral cantilever stiffness k_y and the lateral contact stiffness k_{yc}. The extension of these two springs are y and y_c respectively upon application of a force F_y. (Source: Cain et.al. [28])

The force and deflections may be modeled as shown in Figure 2.3 where F_y is the friction force required to cause slip at the contact interface. It follows that

$$y_s = y + y_c \qquad \textbf{10}$$

and

$$F_y = k_y y_c = k_y y = k_{tot} y_s \; ; \qquad \textbf{11}$$

where y_s is the lateral scanner travel, y_c is the lateral deformation of the contact, and y is the component of the lateral movement at the interface leading to the twisting of the cantilever. In AFM experiments, this twist is recorded by the photodiode. Hence, the LFM signal, V_{LFM}, is equal to

$$V_{LFM} = \zeta \varphi, \qquad \textbf{12}$$

where ζ is a scalar of the lateral photodiode output for a given type of cantilever, and φ is the actual twist in radians experienced by the cantilever.

The combined stiffness, k_{tot}, is given by

$$K_{tot} = (1/k_y + 1/k_{yc})^{-1} \quad \textbf{13}$$

The slope, S, of the LFM output while the surfaces stick is equal to the twist of the cantilever, divided by the travel of the scanner, y_s. That is,

$$S = V_{LFM} / y_s = \zeta \varphi / y_s , \quad \textbf{14}$$

and since $\varphi = y / h$,

$$hS = y \zeta / y_s \quad \textbf{15}$$

Combining eqs [11] and [15] gives

$$hS = k_{tot} \zeta / k_y \quad \textbf{16}$$

The scalar, ζ, and the lateral cantilever stiffness, k_y, are assumed to be constant, so from eq. [16], hS varies with the combined stiffness, k_{tot}. Hence, if conditions can be found in which k_{tot} approaches k_y, a condition in which all the deflection is occurring in the cantilever, ζ would be simply to hS. Since $k_{\varphi} = h^2 k_y$

$$k_{\varphi} = h^2 k_{tot} (1 + y_c/y) \quad \textbf{17}$$

For a given beam twist, y scales directly with h but y_c does not change significantly. Thus, with increasing sphere size, $y_c/y \ll 1$ and $h^2 k_{tot}$ approaches k_{φ}. Because of the asymptotic behavior with larger spheres and higher load conditions, hS under these conditions approximates to the scaling factor ζ. They have also shown this for a stiff AFM cantilever at high normal loads.

As can be seen, all three lateral force calibration techniques differ significantly in terms of their theoretical basis and their implementation. The evaluation of these three techniques in terms of reliability for quantitative friction force microscopy has surprisingly not been reported. The next chapter addresses this issue and presents data obtained using these calibration techniques on a single sample.

CHAPTER 3. Comparison of lateral calibration methods

3.1 Introduction

A primary objective of this research was to determine the lateral force calibration method that is best suited for commercially available Si_3N_4 cantilevers that are commonly used in friction force microscopy. In this chapter, the three widely used calibration methods, namely Ogletree et.al.'s method [27], Ruan and Bhushan's method [26] and Cain et.al.'s method [28], which were explained in the previous sections, are utilized to obtain quantitative friction force data on two engineering surfaces. Interfacial shear stress obtained from the friction data on a biomaterial is compared to values obtained using macroscale methods in order to assess the reliability and suitability of the various calibration methods

3.2 Experimental

Friction force microscopy was performed using a Dimension 3100 AFM (Nanoscope IV, Digital Instruments Veeco Metrology) with commercially available Si_3N_4 cantilevers with integrated probes. Prerequisites for quantitative friction force microscopy are evaluation of normal spring constant and probe radius. Normal spring constants were evaluated using the calibrated lever technique of Tortonese and Kirk [16] as explained below. The probe radius was evaluated to be 44 nm using a TGT01 sample (Mikromasch, USA) and SPIP software (Image Metrology, www.imagemet.com). For the calibration methods, we used a commercially available silicon sample (TGGO1, Mikromasch, USA) that contained regions of ridges of equal slope (55°), used for Ogletree et al.'s method as well as flat regions used

for the other two methods. A 10 μm x 10 μm image of the TGG01 sample is shown in Figure 3.1.

3.3 Results

Normal spring constant determination

Two measurements are required to do normal force calibration. First the cantilever under test is placed under an infinitely hard sample and the cantilever deflection, δ_{tot}, is measured as the substrate is moved vertically. This measurement also establishes the vertical deflection sensitivity of the detector-cantilever setup. Second, the cantilever under test is

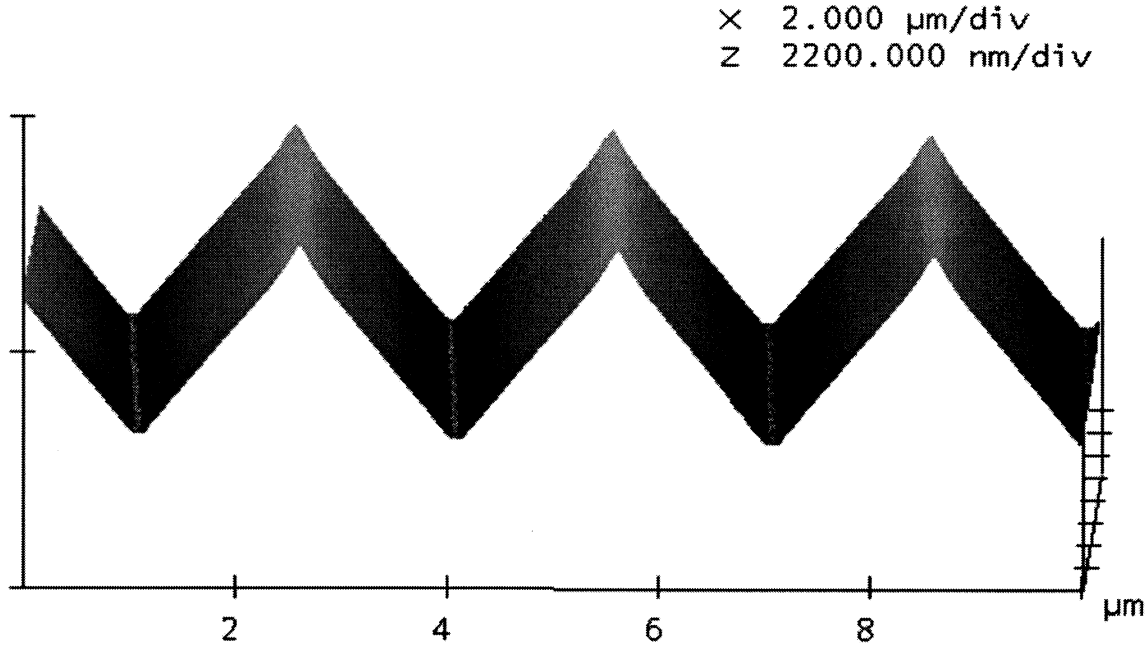

Figure 3.1 10 μm x 10 μm image of the TGG01 sample obtained using a Si_3N_4 in contact mode

placed into contact with the free end of the reference cantilever and the deflection of the cantilever under test, δ_{test}, is measured as the base of the reference cantilever moves vertically by the amount δ_{tot}. If the force constant of the reference cantilever is k_{ref}, then the force constant of the cantilever under test can be calculated as

$$k_{test} = k_{ref} (\delta_{tot} - \delta_{test} / \delta_{test} \cos \theta) \qquad 1$$

where θ is the angle between the cantilever under test and the reference cantilever. This measurement can be accomplished with a standard AFM with force versus distance curve software. In this case, δ_{tot} is the slope of the force-distance curve when the cantilever under test is in contact with a hard surface and δ_{test} is the slope of the force-distance curve when the cantilever under test is in contact with the free end of the reference cantilever. A schematic of the test cantilever in contact with the reference cantilever is shown in Figure 3.2.

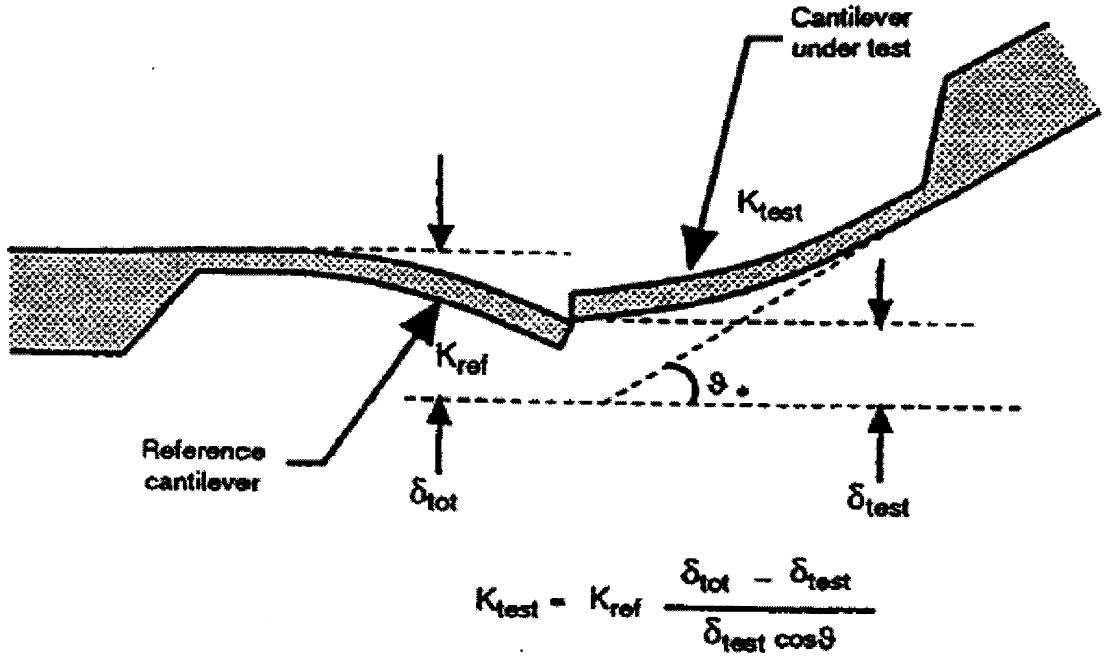

Figure 3.2 Schematic of the calibrated lever technique to measure the normal force constant of cantilevers (Source: Tortonese and Kirk [16]).

Scanning electron microscopy (SEM) image of the reference cantilever that we used is shown in Figure 3.3. The resonant frequency and the Q factor of the reference cantilever were experimentally determined using the AFM. The plan dimensions of the cantilever were calculated from the OM image. The dimensions, resonant frequency and Q factor were used to find the force constant using Sader's method [17]. The value obtained was 0.366 N/m (as opposed to quoted value of 0.283 N/m). This value was used for the normal calibration of all cantilevers used in this thesis work unless otherwise specified. For our cantilever, we obtained a normal spring constant of 0.32 N/m (quoted value was 0.58 N/m).

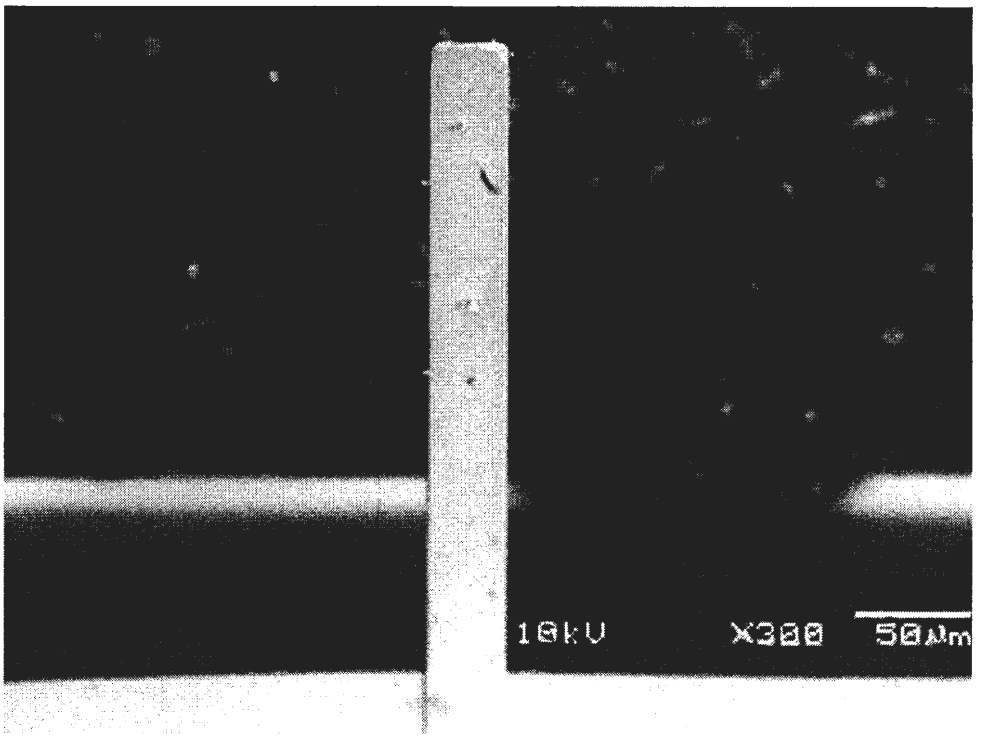

Figure 3.3 Scanning electron microscopy (SEM) image of the reference cantilever. Length and width of the reference cantilever were calculated from this image.

Comparison of lateral force calibration methods

Ogletree et al.'s method:

Experimentally, Ogletree's method is carried out by making the tip scan back and forth along exactly two slopes of a ridge of the silicon sample at a particular scanline. This is done by disabling the fast scan axis in the AFM software. After a specific time interval, the setpoint is increased to a specific amount which essentially increases the normal load. So, for a 512 scanline image with 1 Hz as the scan speed, if the setpoint was increased every 2 seconds, then the load would have been increased 256 times by a constant amount and there would be 256 data points for analysis. In actual experiments, this is done by scanning two slopes of a particular ridge in a direction perpendicular to the long axis of the cantilever and capturing an image of the actual deflection, friction trace and friction retrace signals and importing the image data into a MATLAB code (Source: R.W.Carpick research group, University of Wisconsin, Madison) which averages the subset of points for each facet and calculates the friction loop width and offset for both the upward and downward slopes at various loads and is plotted as a function of normal load. From the plots, the slopes Δ' and W' are determined and used in the equations explained in the previous section to solve for α. If the normal force constant was not calibrated prior to this experiment, then we obtain α/β instead of just α where β is the normal force signal sensitivity.

The plot of friction loop width and offset on upward and downward slope of a particular ridge are shown in Figure 3.4. The slopes of the above plot were used in the equations specified in the discussion of Ogletree's method in the previous chapter to get a calibration factor of 2.16 μN/V.

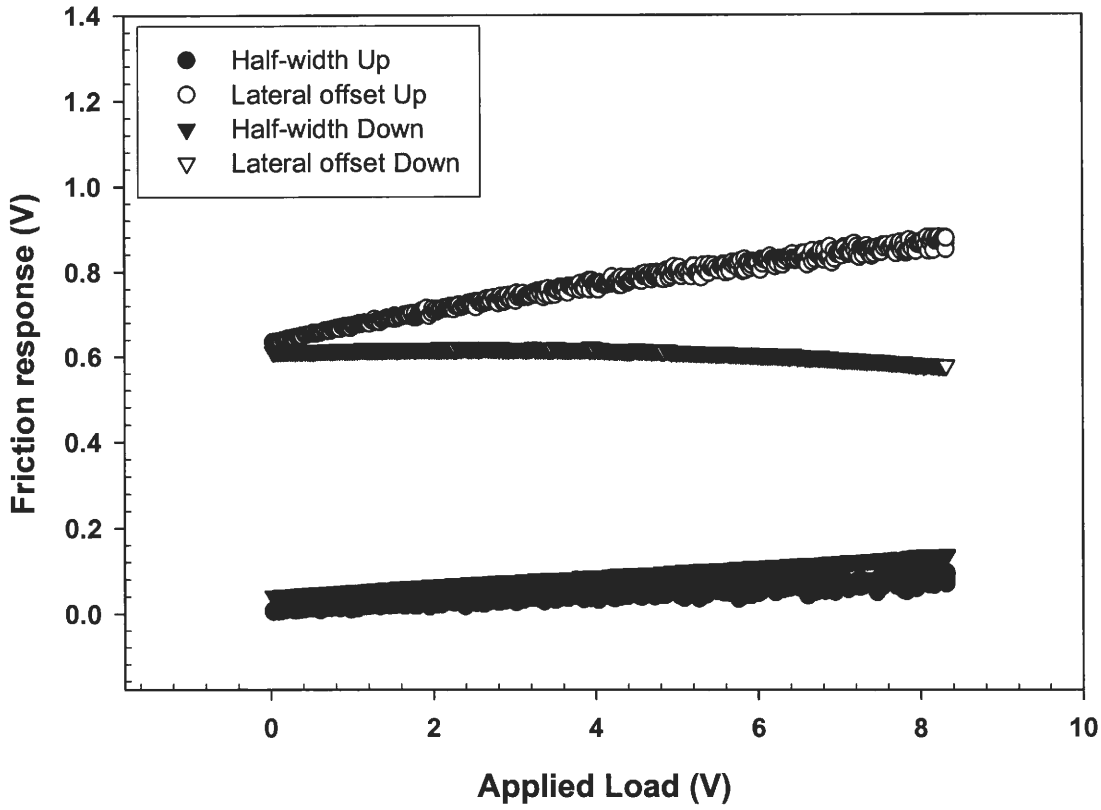

Figure 3.4 Plot of friction loop half-width and offset on upward and downward slopes of a ridge as a function of the applied load

Ruan and Bhushan's method:

In actual experiments in commercial AFMs, Ruan and Bhushan's method can be done in the following way. The tip is scanned back and forth on a particular scanline (by disabling the fast scan axis) in a direction parallel to the long axis of the cantilever and the setpoint is increased in steps. At each step, the height TMR(trace minus retrace) and the Z center position is noted down. These values are plotted as a function of normal load. Such a plot for silicon nitride tip on a silicon wafer is shown in Figure 3.5.

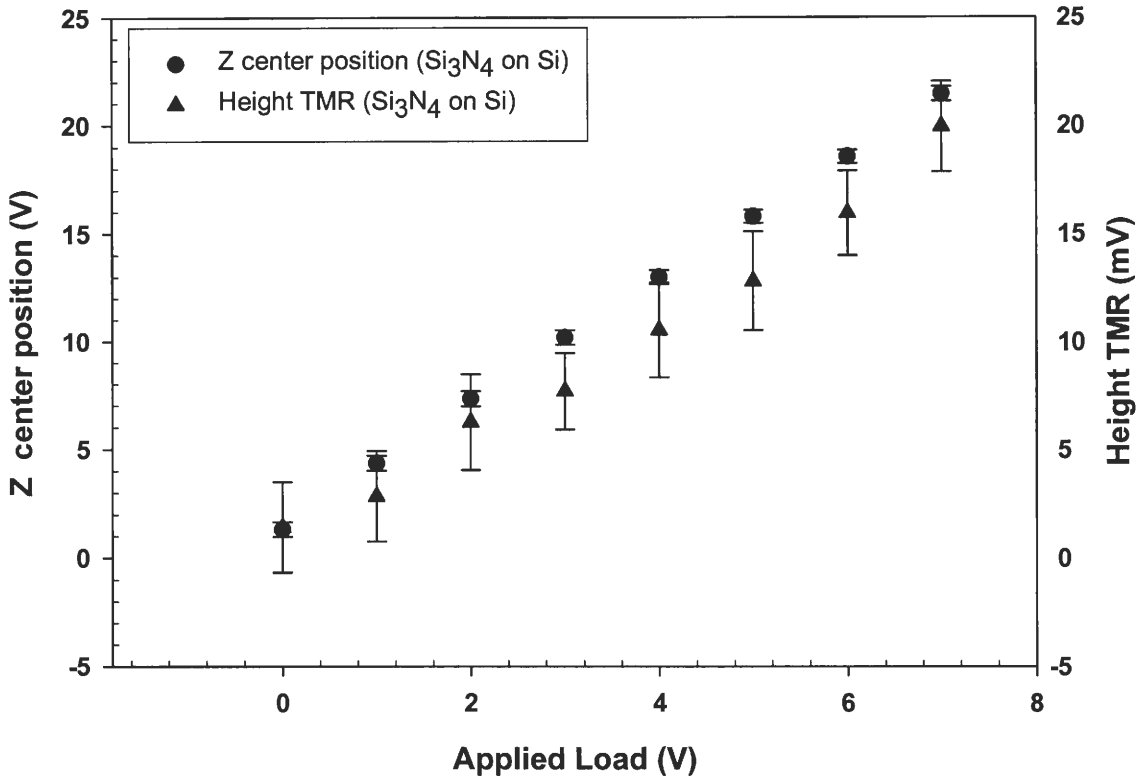

Figure 3.5 Variation of ($\Delta H_1 + \Delta H_2$) (represented by height TMR) and H_0 (represented by z center position) as a function of applied load for a Si_3N_4 cantilever on Silicon.

The slopes of these plots represent $\Delta (\Delta H_1 + \Delta H_2) / \Delta NF$ and $\Delta (H_0) / \Delta NF$ where NF is the normal force or the applied load. Hence, the equation 15 can be modified as

$$\mu = W_f / W_0 = \Delta (\Delta H_1 + \Delta H_2) / \Delta NF * \Delta NF / \Delta (H_0) * L / (2\,l) \qquad 2$$

Substituting the values of the slopes of plots from Figure 3.5 and measured plan dimension parameter L (115 microns) and probe height l (3 microns) from manufacturer's specifications in equation 2, the coefficient of friction was calculated to be 0.017.

In the experiments where the tip is scanned perpendicular to the long axis of the cantilever, the lateral response of the cantilever is noted down as a function of applied normal

load. This is done by scanning the tip back and forth on a same scan line by disabling the fast scan axis and increasing the setpoint in steps and noting down the friction TMR (friction signal in an AFM). This plot of friction force in millivolts as a function of applied normal load (in nanonewtons) is shown in Figure 3.6.

The slope of this plot is 1.115 mV/nN which is equated to the coefficient of friction obtained in the previous approach where the tip was scanned parallel to the long axis of the cantilever. On equating the two, we get a lateral calibration factor of 15.58 nN/V. This value is comparable to the value of 8.7 nN/V which was reported for a Si_3N_4 tip of force constant 0.4 N/m scanning on a Pt surface [26].

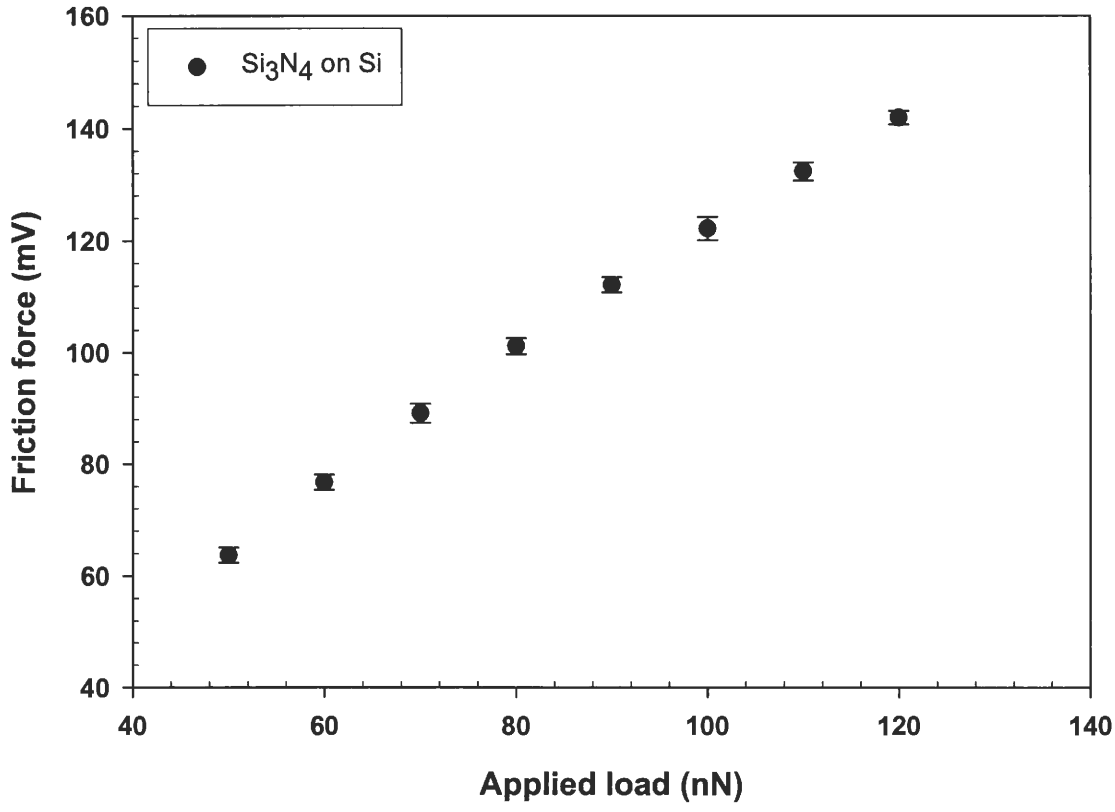

Figure 3.6 Variation of friction force (represented by friction TMR) as a function of applied load for a Si_3N_4 cantilever on Silicon.

Cain's method:

For the cantilevers that we used and load range we were working in, Cain's method did not seem to yield a good result as we were under the load regime where the effect of lateral contact stiffness was still significant. We carried out the experiments on silicon at various normal loads ranging from 10 nN to 80 nN. The slope of the stick portion of every friction loop (taken at various loads) was calculated and they were plotted against the applied normal load. The plot is shown in Figure 3.7. The data shows that for the Si3N4 cantilevers we used, obtaining a single lateral calibration factor is not possible.

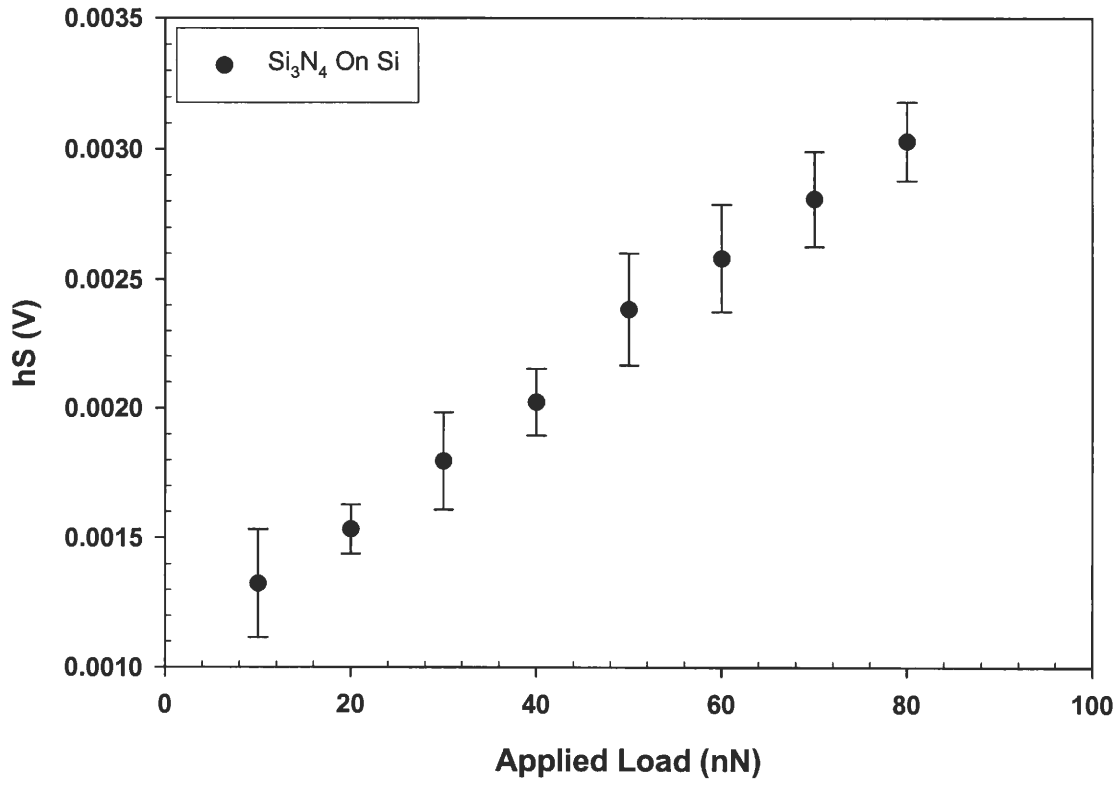

Figure 3.7 The slope of the stick portion (S) of a friction loop as a function of applied load.

Table 1 summarizes the results of Ogletree et al.'s and Ruan and Bhushan's method. Cain's method did not yield a single value of the lateral calibration constant and is therefore not listed. There is an order of magnitude difference in the COF and calibration factor between the two methods on the same sample. The probe shape and size was verified to be predominantly unchanged throughout our experiments. Care was taken to ensure the assumptions and precautions associated with each technique were complied with.

Table 1: Comparison of data: lateral calibration methods

Method	Coefficient of friction on Si	Calibration factor (nN/mV)
Ruan and Bhushan	0.017	0.0156
Ogletree et.al.	0.307	2.288 ± 0.054

In order to obtain a better sense of which method yields a more reasonable number, the friction response of an engineering material whose macroscale interfacial shear strength is known was measured. By comparing the interfacial shear strength values obtained from friction force microscopy data using both the calibration methods against the known value, a better understanding of the reliability of each technique can be obtained. The material chosen was ultra-high molecular weight polyethylene (UHMWPE), a biomaterial used in joint implants. Macroscale measurements for this material report a value of 2 - 7 MPa [33]. The uncalibrated friction data obtained on UHMWPE is shown in Figure 3.8.

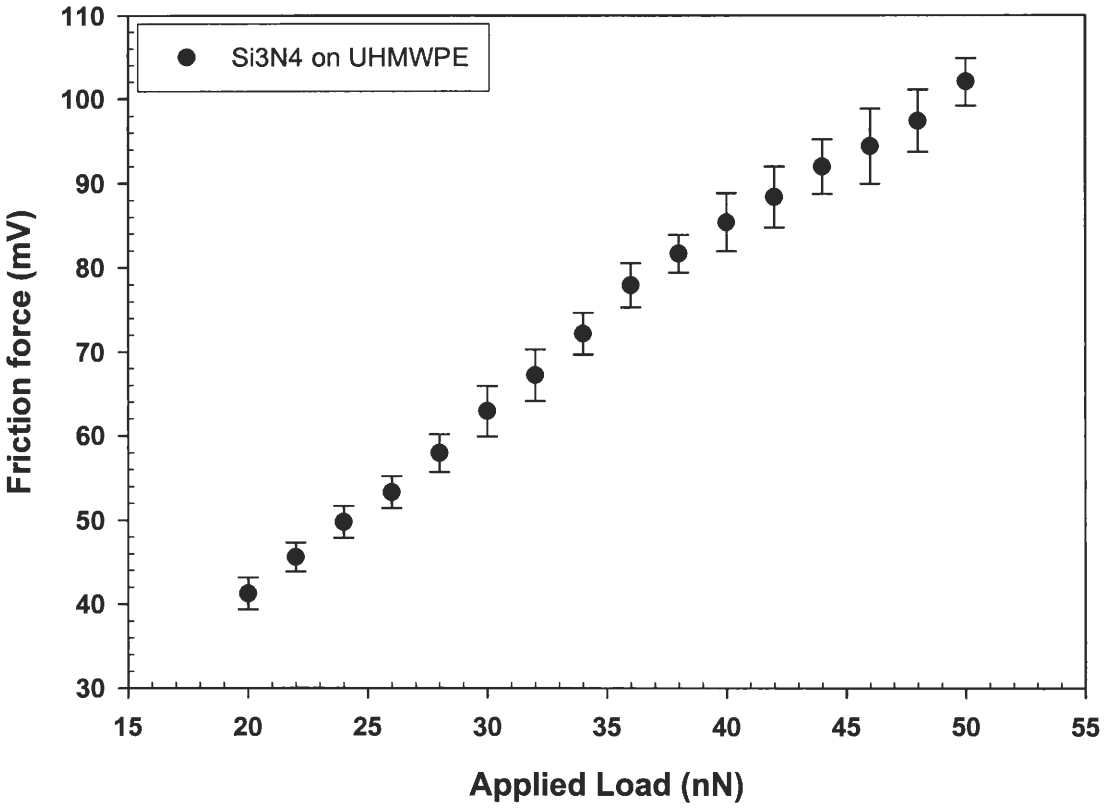

Figure 3.8 Friction force vs applied load – Si_3N_4 cantilever on a UHMWPE sample

After converting the data to quantitative friction force values, the interfacial shear strength of the material pair can be calculated from the friction force data by using an appropriate contact mechanics model [34; 35] or using advanced techniques that do not rely on contact mechanics [32; 36] as described below.

In this study, the Johnson-Kendall-Roberts (JKR) contact model [37] is employed for characterization of the shear strength of UHMWPE. The JKR model is suitable for soft samples with low elastic modulus which is appropriate for UHMWPE. The general features of the JKR theory are as follows. Surfaces are considered to possess a finite surface energy

per unit area $\gamma = \gamma_1 + \gamma_2 + \gamma_{12}$, where γ_1 and γ_2 are the respective surface energies and. The contact area A as a function of externally applied load L is given by

$$A^{\frac{3}{2}} = \frac{\pi^{\frac{3}{2}} R}{K}.\left[L + 3\pi R\gamma + \sqrt{6\pi R\gamma L + (3\pi R\gamma)^2}\right], \qquad \mathbf{3}$$

where R is the tip radius, γ is the interfacial energy and K is the reduced modulus of the two materials, is given by

$$K = \frac{4}{3}\left(\frac{1-\upsilon_1^2}{E_1} + \frac{1-\upsilon_2^2}{E_2}\right)^{-1}, \qquad \mathbf{4}$$

with E_1 and E_2 the respective Young's moduli, and υ_1 and υ_2 the respective poisons ratios. At zero applied load, there is a finite contact area given by

$$A_o = \pi\left(\frac{6\pi\gamma R^2}{K}\right)^{\frac{2}{3}}. \qquad \mathbf{5}$$

Furthermore, a finite negative load is required to separate the surfaces. This value is often referred to as the critical load and is given by

$$L_c = -\frac{3}{2}\pi R\gamma. \qquad \mathbf{6}$$

This is equivalent to the pull-off measured in AFM experiments (if the tip is truly parabolic). From the pull-off forces, one can evaluate the interfacial energy. At the critical load, a finite contact area exists. Frictional force F_f is directly proportional to the contact area, i.e.,

$$F_f = \tau A, \qquad \mathbf{7}$$

where τ is the interfacial shear strength. By substituting the expression for the contact area from Equation 3, we can determine the interfacial shear strength provided we can get quantitative friction data as a function of applied normal load.

The value thus obtained for UHMWPE using Ruan and Bhushan's calibration factor was 5.85 MPa. The value obtained using Ogletree's method resulted in a shear strength of 0.86 GPa. Macroscale measurements report a value of 6.95 MPa [33]. Interfacial shear strengths for a diamond-tungsten carbide interface in vacuum has been reported to be about 240 MPa [38]. Clearly Ruan and Bhushan's method results in a more acceptable value since it is unreasonable to expect a soft polymer to exhibit higher shear strength than an interface between hard materials in vacuum.

3.4 Conclusions

In this study, we analyzed three lateral calibration methods on a common sample (Silicon) and used the calibration factors to quantify the frictional force for a UHMWPE-Si_3N_4 interface and corresponding interfacial strength of the contact. All three lateral calibration methods were relatively time-consuming when compared to normal calibration methods. Ogletree's method involves scanning a two-sloped sample at different loads and analyzing the data using custom written MATLAB code and further numerical calculations to determine the calibration factor. Shear strength values of UHMWPE obtained using this method is two orders of magnitude higher than literature values. It appears therefore that for the Si_3N_4 cantilevers used in this study, Ogletree et al's method does not yield reliable calibration factors.

RB's method involved scanning in both directions (parallel and perpendicular) to the long axis of the cantilever and obtaining lateral response in both cases. The data was then analyzed via simple graphing. Though both these methods consumed the same amount of

time as far as the experiment and analysis goes, Ruan and Bhushan's method is more straightforward and less cumbersome. Moreover, the values obtained for the shear strength of UHMWPE calibrated using Ruan and Bhushan's method was comparable to the literature values. This suggests that Ruan and Bhushan's method is viable for lateral calibration for the Si_3N_4 cantilevers used in this study. Cain's method is not applicable for the Si_3N_4 cantilevers used in this study as there is a significant dependence of the contact stiffness on the normal load.

CHAPTER 4. Effect of protein adsorption on the friction behavior of ultra-high molecular weight polyethylene (UHMWPE)

4.1 Background and motivation

Total joint replacement (TJR) or arthroplasty represents a significant advance in the treatment of painful and disabling joint pathologies. TJR is a surgical procedure in which certain parts of an arthritic or damaged joint, such as a hip or knee joint, are removed and replaced with a plastic or metal device called prosthesis. The prosthesis is designed to enable the artificial joint to move just like normal, healthy joint. It can be performed on any joints of the body including the hip, knee, ankle, foot, shoulder, elbow, wrist, and fingers. Of these procedures, the hip and knee total joint replacements are by far the most common. A typical hip joint prosthesis is shown in Figure 4.1.

TJRs have proved to be one of the most successful applications of biomaterials over the last 30 years. Currently, over 1 million devices are implanted annually in patients worldwide and they have resulted in significant restoration of function and reduction of pain in approximately 90% of patients [39]. As successful as most of joint replacement procedures are, the artificial joints can become loose and unstable during use, requiring a revision surgery (surgery to replace a failed replacement joint). Figure 4.2 shows the projection of primary and revision total joint arthroplasty in the United States clearly addressing the issue of tribology in TJRs is of great importance to human health and economy. It has only been in the last decade that it has become recognized that tribology (wear) is the major cause of long

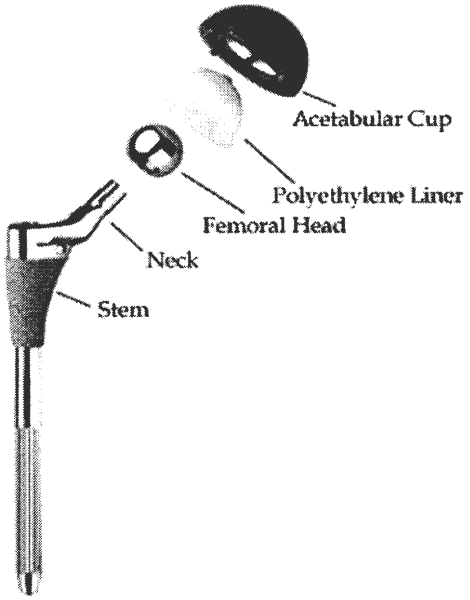

Figure 4.1 Exploded view of a typical hip implant prosthetic. (Source: Bozic, Rubash, et. al, Modes of Failure in Revision Hip and Knee Replacement)

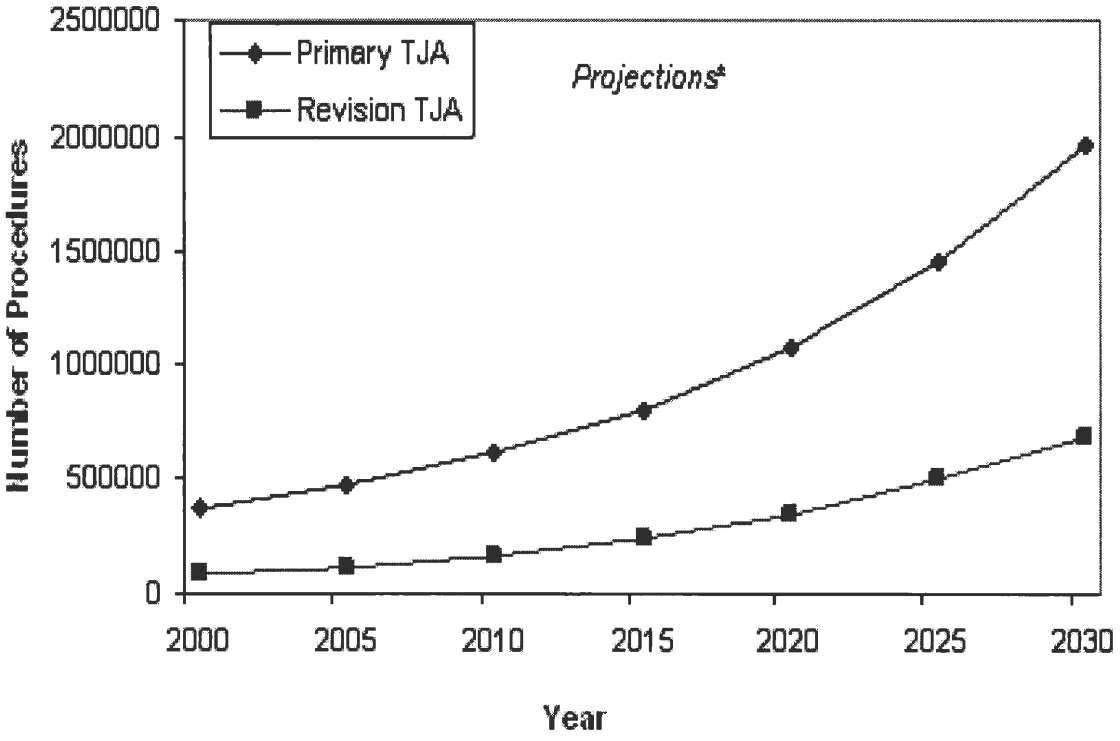

Figure 4.2 Projection of primary and revision TJR procedures performed in the US (Kevin J. Bozic et.al., www.cdc.gov)

term failure of joint replacements. Specifically, the tribological issues, friction and wear at interface between the femoral head (usually a hard metal alloy) and acetabular cup lining (usually a soft polymer) and the fretting corrosion at the interface between the head and stem.

4.2 Materials in TJRs

Many different material pairs have been used for TJRs. The major materials are briefly discussed below.

- Stainless steel was used by Sir John Charnley [40] in his work and is usually used against plastic. He originally selected PTFE (Teflon) as an ideal pairing for stainless steel, and good results were expected due to the low friction observed with the pair; however, wear was extremely high and biocompatibility was low. He then replaced Teflon with UHMWPE and much improved wear and better biocompatibility was seen.
- Cobalt Chromium (CoCr) is also used with UHMWPE or with itself due to its excellent corrosion resistance in the body. It also shows very good wear resistance.
- Titanium used with UHMWPE was introduced in the late 1970's but was eventually found to be inferior to the performance of CoCr.
- Alumina paired with itself shows good wear characteristics, and when paired with UHMWPE generally shows some improvement over CoCr.
- Zirconia is used due to its increased strength over alumina; however it is also much more expensive.

Sir John Charnley's introduction of UHMWPE as an alternative to Teflon proved to be such a good choice that it is the still the "only suitable polymer material for hip joint cups, even after more than 30 years" [41]. Its performance compared to other polymers is shown in Table 1.

Table 1. Mean clinical linear wear rates of polymer cup materials. [42]

Material	Wear Rate
PTFE	3.3 mm/yr
Polyester	0.5 mm/yr
Delrin	0.2 mm/yr
UHMWPE	0.07 mm/yr

This combination of materials has proved to be extremely successful, giving low friction, low wear rates of the UHMWPE and smaller amount of wear debris, which could be tolerated by the body. Although UHMWPE has a wear rate lower than many other materials, the average lifetime of artificial hip joints incorporating the polymer are only 15-20 years. Considerable amount of research is being devoted to increasing the wear life of the prosthesis.

Due to the high contact area between the cup and liner, the friction and wear mechanisms are generally adhesive in nature at the onset of operation, especially in hip joints, where maximum principal stresses are much less than the yield strength of the UHMWPE [43]. However at later stages, loosening and particulate debris compound the wear. Hence, it is of interest to minimize adhesive contributions to friction and wear in TJRs.

4.3 Boundary lubricants in TJRs

The human joint operates in the presence of a physiological fluid known as the synovial fluid. The natural lubricant, called synovial fluid, is a clear, viscous fluid which serves three purposes: it lubricates the articulating surfaces, carries nutrients to the cartilage cells, or chondrocytes, and transports waste products away from the cartilage. The synovial membrane, which surrounds the joint, serves several purposes: it regulates the amount and content of the synovial fluid, it removes waste materials from the synovial fluid and allows nutrients to enter the synovial capsule, and it secretes synovial fluid and other macromolecules for lubrication of the joint [44]. A diagram of a simplified synovial joint is shown in Figure 4.3.

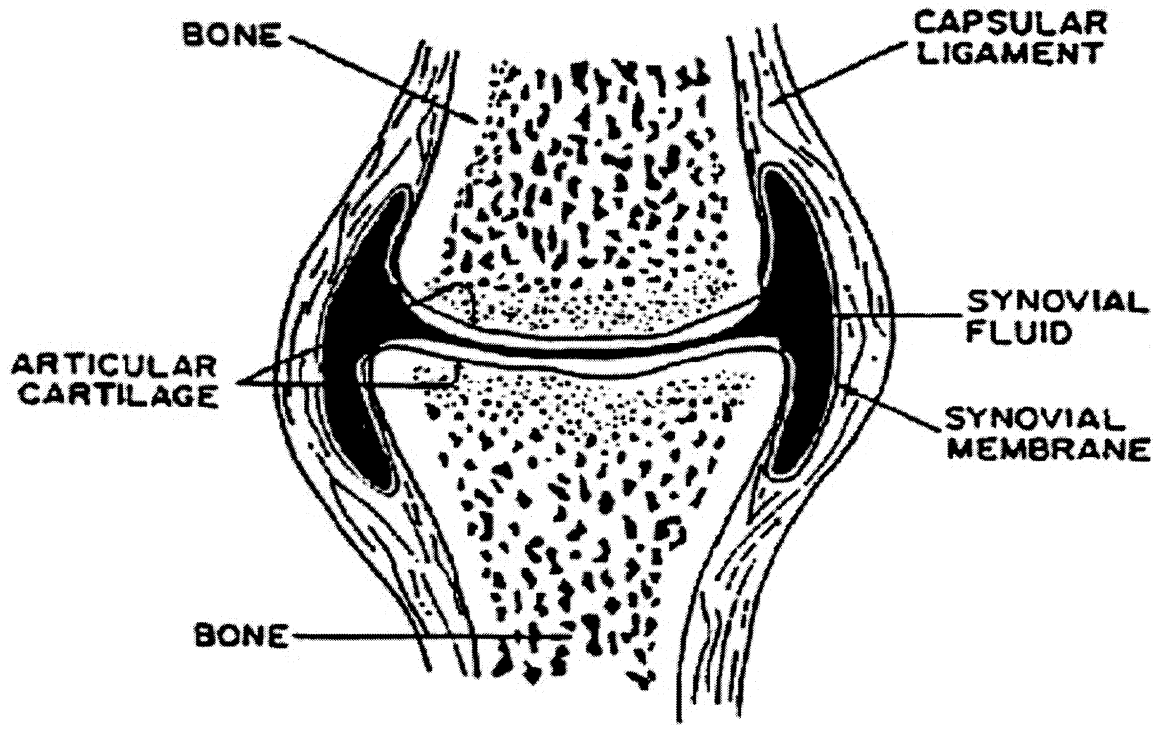

Figure 4.3 A synovial joint (Source: Michael C. Owellen, Biotribology: The effect of lubricant and load on articular cartilage wear and friction)

It is recognized that the synovial fluid contains various kinds of serum proteins, hyaluronic acid and also various kinds of lipids [45]. It is generally believed that the synovial fluid acts as a boundary lubricant to the joint interface and helps to minimize friction and wear. It has been found that albumin constitutes to almost 60% of the total protein concentration in serum and synovia [45]. Hyaluronic acid is a kind of polysaccharide which is responsible for the viscous nature of the synovial fluid [46]. As a result of numerous studies to identify an alternate physiological fluid for use in experiments *in-vitro*, ASTM (American society for testing and materials) has established that the use of bovine serum albumin is acceptable for TJR biomaterials testing. Several studies have attempted to elucidate the role of BSA in the tribology of the cup-head interface in TJRs.

4.4 Effect of BSA constituents on tribological behavior of UHMWPE

Sawae et.al.[45] have studied the effect of two different synovial constituents (albumin and hyaluronic acid) on the friction and wear of UHMWPE using a pin-on disk apparatus and have shown that proteins affect the friction and wear quite drastically than the other constituents. Heuberger et.al.[47] and Widmer et.al.[48] have shown that rendering the polymeric surface more hydrophilic modifies the protein adsorption behavior of albumin and enhances the boundary lubrication behavior of bovine serum albumin. Though there are many studies on the tribological aspect of BSA on polymers using sophisticated joint simulators and tribometers, there are only a few which has realized the efficacy of atomic force microscopy to study the tribological behavior of bovine serum albumin on polymers. Park et.al. [49] have studied both macroscopic and microscopic (using AFM) friction measurements on bovine articular cartilages and shown that the microscale and macroscale

friction coefficient exhibited no statistical differences and that AFM could be used to explore the role of boundary lubricants in cartilages and provide greater insight into design of biomaterials. Ho et.al. [50] have used atomic force microscopy to study the wear mechanism and eventual failure of UHMWPE insert in TJR prosthesis.

4.5 Studies on adsorption mechanism of proteins

Widmer et.al.[48] have also shown that the adsorption mechanism of proteins onto polymeric surfaces is important to the friction behavior. The mechanism of adsorption of proteins onto polymeric surface has been researched extensively in the past using various other techniques too. Van Straaten et.al.[51] used attenuated total reflectance – Fourier transform infrared (FTR-FTIR) spectroscopy to study the adsorption of bovine serum albumin on various polymeric surfaces such as Poly(vinyl chloride), Poly(vinyledene fluoride), poly(methylmethacrylate) and poly(ethylene glycol)-grafted PMMA surfaces and showed that PEG surfaces exhibited the lowest albumin adsorption. Xu et.al. [52] used adsorption-desorption techniques, FTIR analysis and streaming potential measurements to arrive at a physical model for adsorption of BSA on polyethylene membranes. Balcells et.al [53] have quantified the protein adsorption on polymeric surfaces using enzyme-linked immunosorbent assay with radiolabeling techniques. Few other researchers have used Optical wave guide spectroscopy (OWLS) to quantify the amount of proteins adsorbed on the surface.

4.6 Research objectives

It is of importance to know how the tribological characteristics of UHMWPE change as soon as the TJR comes in contact with the physiological fluid. There is also a paucity of data to show how BSA constituents affect the interfacial shear strength of UHMWPE, which can provide insights into controlling the adhesive friction and wear. For example, friction performance of UHMWPE as a function of exposure time to bovine serum albumin has not been studied to date. The use of atomic force microscopy as a tool for nanotribology of prosthesis can be exploited for the quantification of shear stress for the biomaterial interface. These form the motivation behind this study.

The main objective of this study is to observe and quantify the friction response of UHMWPE (using atomic force microscopy) as a function of (1) exposure time in bovine serum and (2) concentration of bovine serum. Consequently, from friction theories, interfacial shear strength for these soaking times and concentrations are also calculated and compared. Additionally, fluorescence microscopy and contact angle measurements have been performed as a function of exposure time to bovine serum albumin to report any correlation between the adsorption of serum proteins and the friction behavior.

4.7 Experimental

Materials:

UHMWPE samples were prepared from bar stock obtained from K-Mac Plastics (Grand Rapids, Michigan). Bovine serum (Lot No. 518424, molecular weight 69,000, isoelectronic point (IEP) 4.9) was obtained from Sigma-aldrich and used without further treatment for friction studies. For friction measurements, bovine serum which had a initial

protein concentration of 72 mg/ml was diluted to 10 vol% and 60 vol% with distilled water and 0.3 wt% sodium azide [45] was added to the diluted bovine serum to retard bacterial growth.

AFM observations:

AFM experiments in contact mode were carried out with a Dimension ™ 3100 AFM (Nanoscope IV, Veeco Instruments, Santa Barbara, CA) in controlled low humidity (10 ± 4 % RH) conditions to minimize effects of adsorbed water vapor. Standard V-shaped silicon nitride probes from Veeco with a quoted normal spring constant of 0.58 N/m and tip radius of 10-40 nm were used. The normal spring constant of the cantilever used was calibrated using the technique described by Tortonese and Kirk [16] and found to have an actual value of 0.23 N/m. The pull-off (adhesive) force, $F_{PO,}$ between the Si_3N_4 tip and the UHMWPE was measured before and after each test from force-displacement curves.

For friction measurements, the probe was scanned perpendicular to the long axis of the cantilever. The friction response of the probe on the sample was taken to be the difference between the lateral deflection values of the forward and reverse scans of a given scan line (i.e. from the friction loop of a scan line). This method is commonly used to eliminate contributions to the lateral deflection signal from non-friction sources [1]. Normal loads were varied from 20 – 60 nN, corresponding to a range of 0 – 6 F_{PO}. Friction force and adhesive force data presented are averages of six measurements at multiple sample locations. The friction force was calibrated using Ruan and Bhushan's method [26] as explained in the previous chapter. The lateral force calibration factor for the tip used was 55.73 nN/V.

The radius of the tip was characterized before and after the experiments using the procedure described in section 1.4 of chapter 1. The images were analyzed using SPIP software (Image Metrology) to calculate the tip radius. The tip profiles were generated using a MATLAB code (shown in Appendix).

Fluorescence measurements:

Protein adsorption onto UHMWPE as a function of exposure time and concentration was qualitatively measured using fluorescence microscopy. For the fluorescence microscopy studies, bovine albumin tagged with fluorescein isothiocyanate (FITC) dye (Sigma-Aldrich, Cat. No. A9771), Phosphate-buffered saline (PBS) solution of pH 7.4 (1X) (Invitrogen, Cat. No. 10010-023), Sodium azide (Sigma-Aldrich, Cat. No. 71289) were used as received. For fluorescence experiments, the BSA-FITC dye was dissolved in PBS-1X (pH 7.4) buffer to a concentration of 7.2 mg/ml (BSA) and 43.2 mg/ml (BSA) representing 10 vol% and 60 vol% dilution as used in friction experiments.

UHMWPE samples were soaked in these solutions. They were taken out at different time intervals, then rinsed with de-ionized water and dried with nitrogen gas. They were viewed under a confocal fluorescence microscope with a FITC filter with an allowing wavelength of 492 ± 9 nm. The FITC dye fluoresces at a wavelength of 495 nm and has a very short half-life. Hence, fluorescence images were collected on 2 different locations on each sample within a time period of one minute. The exposure time and gain settings were kept constant for all measurements to ensure the valid comparison of pixel intensity across different samples. These images were imported into ADOBE Photoshop software, where regions of interest were selected on the image and a histogram analysis of the pixels of the

selected region was carried out. From the histogram, the average image intensities were calculated.

Contact angle measurements:

Hydrophobicity of the UHMWPE as a function of exposure time to BSA was measured using contact angle measurements. The contact angle was measured by taking high magnification digital pictures of the droplets on sample using a CCD camera. The pictures were imported into image analysis software (Scion Image) and the contact angles were measured. A schematic of the contact angle measurement is shown in Figure 4.4. The angle θ in the Figure below is the contact angle made by the droplet on the substrate.

4.8 Results

Figure 4.5 shows the friction response of the UHMWPE – soaked in bovine serum and taken out at different time intervals – as a function of applied normal load for various soaking times in BSA. The response of the unsoaked (0 min) sample is also shown. For

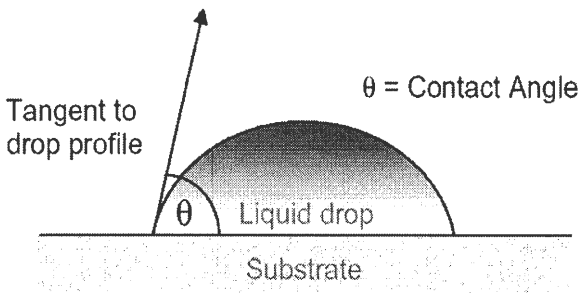

Figure 4.4 Schematic of contact angle measurement

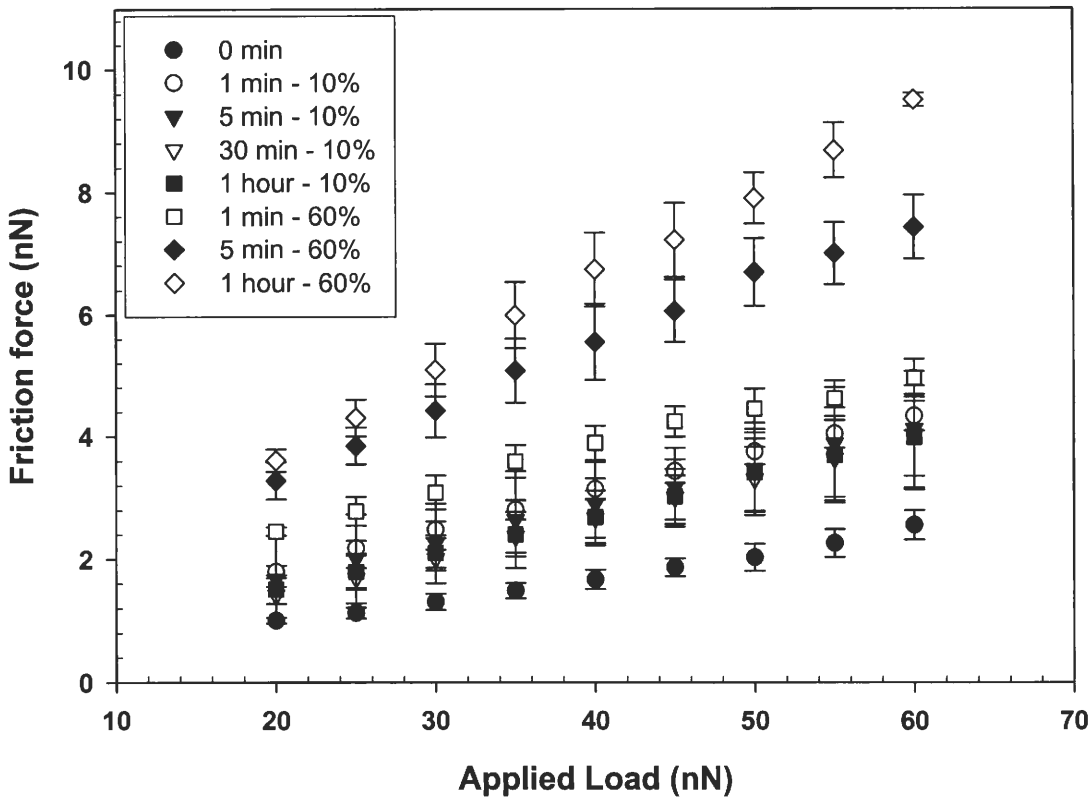

Figure 4.5 Friction force as a function of applied load on UHMWPE soaked in bovine serum for different time intervals at two different concentrations.

all samples, friction force increases with an increase in normal load. For both the 10 vol% and 60 vol% dilutions, the friction force is higher than the dry unsoaked UHMWPE sample. Amongst the 10 vol% dilution samples, the soaking time does not seem to affect the friction significantly. For the 60 vol% dilution, the friction force is significantly higher than the unsoaked UHMWPE and the 10 vol% dilution samples. Also, the soaking times seems to have a considerable effect on the friction in the case of 60 vol% dilution samples. The friction response increases significantly as the soaking time is increased, for 60 vol% diluted solutions. A soaking time of 60 minutes showed the highest friction response and soaking time of 1 minute showed the lowest friction response.

Since no surface damage was seen during testing, the predominant mechanism during the AFM friction experiments is assumed to be adhesive. The adhesive friction is given by:

$$F_a = \tau A_r \qquad 1$$

where τ is the interfacial shear strength, and A_r is the real area of contact. A change in the friction response can therefore be attributed to a change in the real area of contact or in the interfacial shear strength. In our experiments between a hard Si_3N_4 probe and a relatively soft polymer surface, the contact conditions are best described by the Johnson-Kendall-Roberts (JKR) model[37]. In this model, for a given material pair, the contact area is dictated by the probe radius and the work of adhesion between the probe and the sample.

The probe radius was closely monitored before and after each experiment using the calibration samples as described in section 1.4. Figure 4.6 shows probe profiles before (a) and after (b) all experiments.

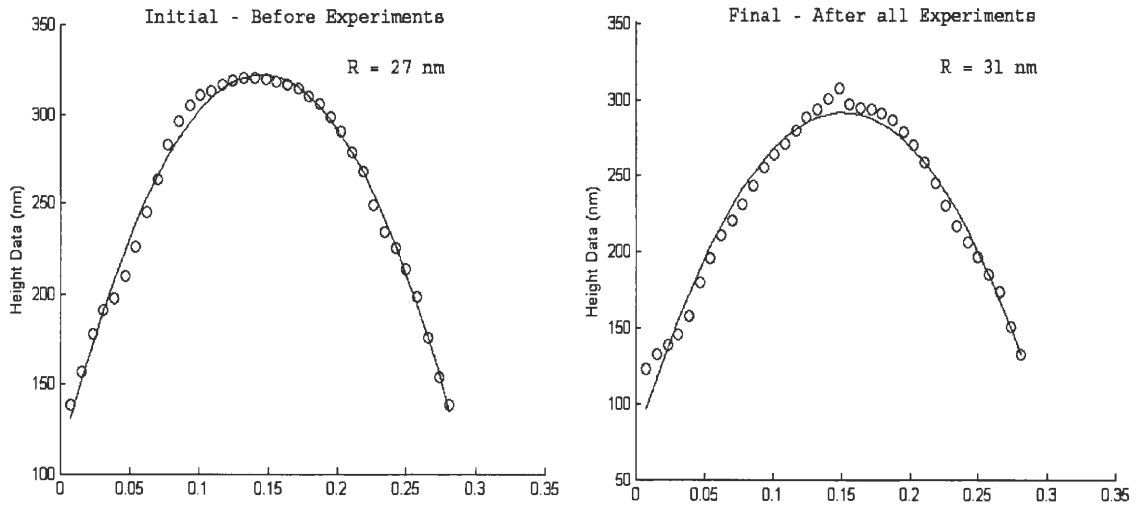

Figure 4.6 Tip profile before experiments (left) and after experiments (right). The tip radius changed slightly from 27nm to 31nm.

The overall change in probe radius was 4 nm, which is about 15% and too small to cause the observed change in friction force.

The work of adhesion was measured from pull-off forces (F_{PO}) for various samples from the equation derived from JKR analysis:

$$F_{PO} = -3/2\ \pi\ R^{*}\ W_{12} \qquad 2$$

Since our experiments were carried out in dry conditions, one can assume that the adhesion component dominates over capillary contributions and that W_{12} can be estimated quite reliably from Equation. 2. Figure 4.7 shows W_{12} to be quite comparable for various samples.

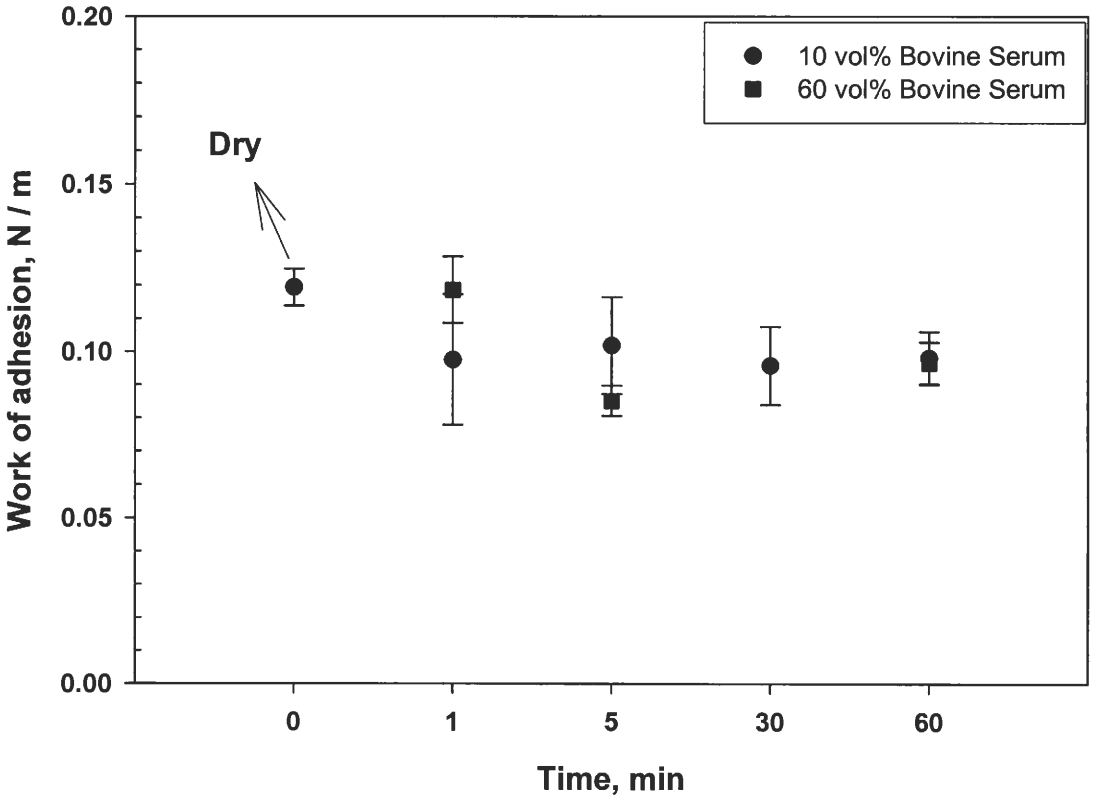

Figure 4.7 Work of adhesion, W_{12}, as a function of soaking time in BSA at two different concentrations

The above findings suggest that the observed friction changes are due to changes in interfacial shear stress. The interfacial shear strengths for various samples were calculated from the friction force by plotting the friction force against the real area of contact (A_r) which was calculated using JKR theory for the various normal loads. The calculated shear strength for all the samples are plotted in Figure 4.8. The shear strength follows the same trend as that of friction response, namely exposure to BSA solutions results in an increase in the interfacial strength of UHMWPE. The dry UHMWPE showed the least shear strength value of 8.68 MPa whereas the highest shear strength of 33.27 MPa was observed on the 60 vol% sample which was soaked for 1 hour.

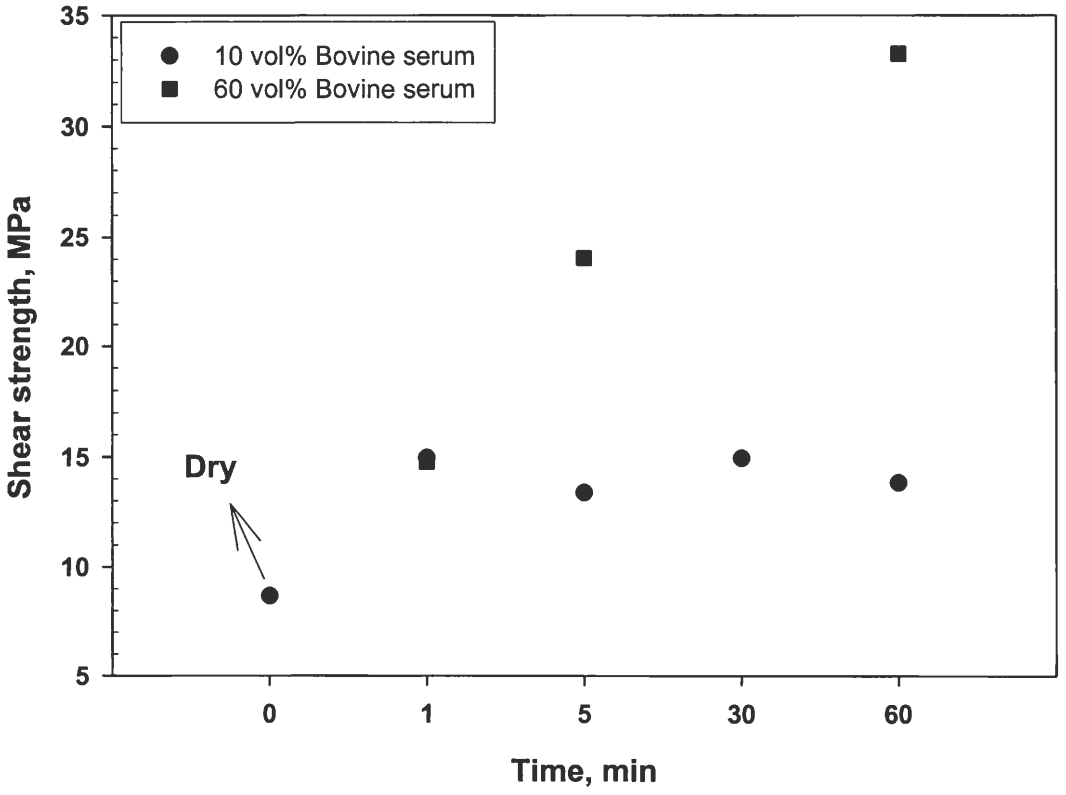

Figure 4.8 Shear strength of the Si_3N_4- UHMWPE interface at different soaking time in bovine serum and at different concentrations of the bovine serum

It is of interest to note that while the shear strength increases with exposure time for the 60 vol% solution, it appears to be independent of soaking time for the 10 vol% solution.

Fluorescence measurements for the various BSA soaked samples are shown in Figure 4.9. UHMWPE samples soaked in 60 vol% BSA solution clearly show higher fluorescence and hence exhibit more protein adsorption than the corresponding 10 vol % soaked samples at all time intervals. For the 10 vol% samples, soaking time did not appear to significantly affect the protein adsorption as the fluorescence intensity remains more or less comparable whereas for the 60 vol% samples, there is a slightly increasing trend of fluorescence with soaking time indicating that more proteins are getting adsorbed as time progresses.

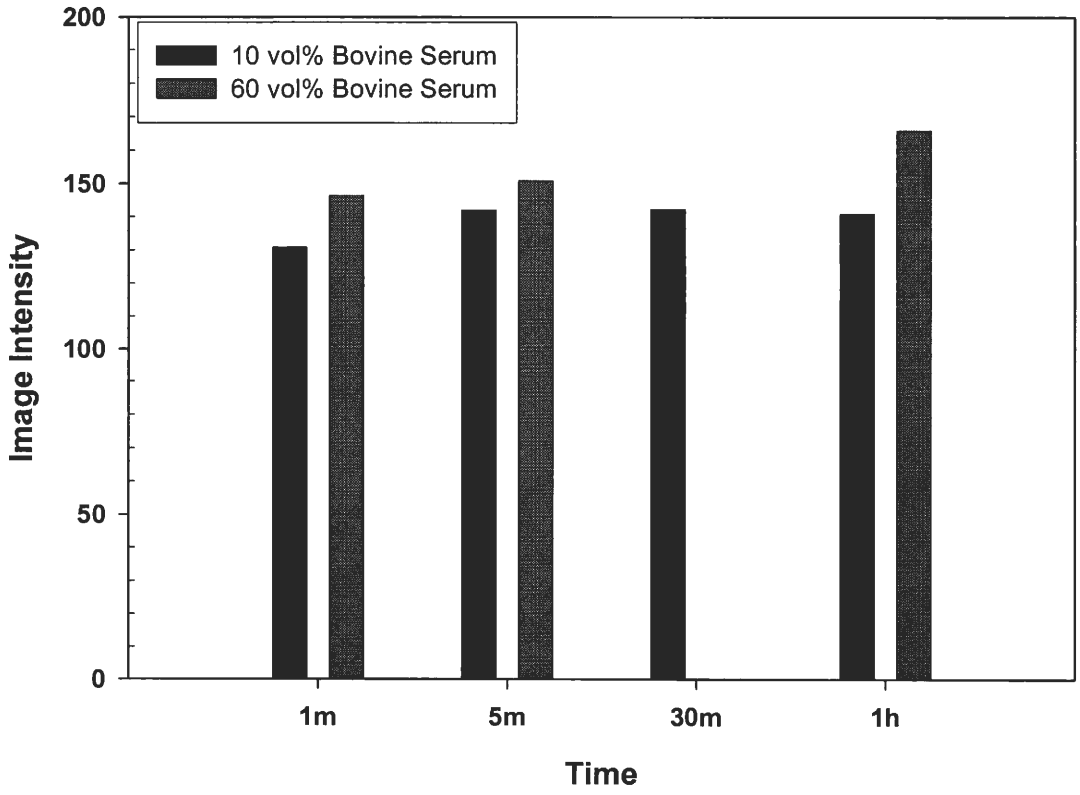

Figure 4.9 Fluorescence image intensities of UHMWPE plotted as a function of soaking time in bovine serum at two different concentrations of the bovine serum

The fluorescence data correlated fairly well with the interfacial shear strength data indicating that the interfacial shear strength of UHMWPE is proportional to the amount of adsorbed protein on the surface.

The contact angle measurements on all samples are plotted in Figure 4.10. A contact angle of 111° was observed on the dry, unsoaked UHMWPE indicating that it is hydrophobic whereas the 60 vol% sample which was soaked for 1 hour showed a contact angle of 29° indicating that it is strongly hydrophilic. The presence of proteins therefore seems to render the sample hydrophilic. This data correlates very well with the interfacial shear strength data. The shear strength increases with a decreasing level of hydrophobicity.

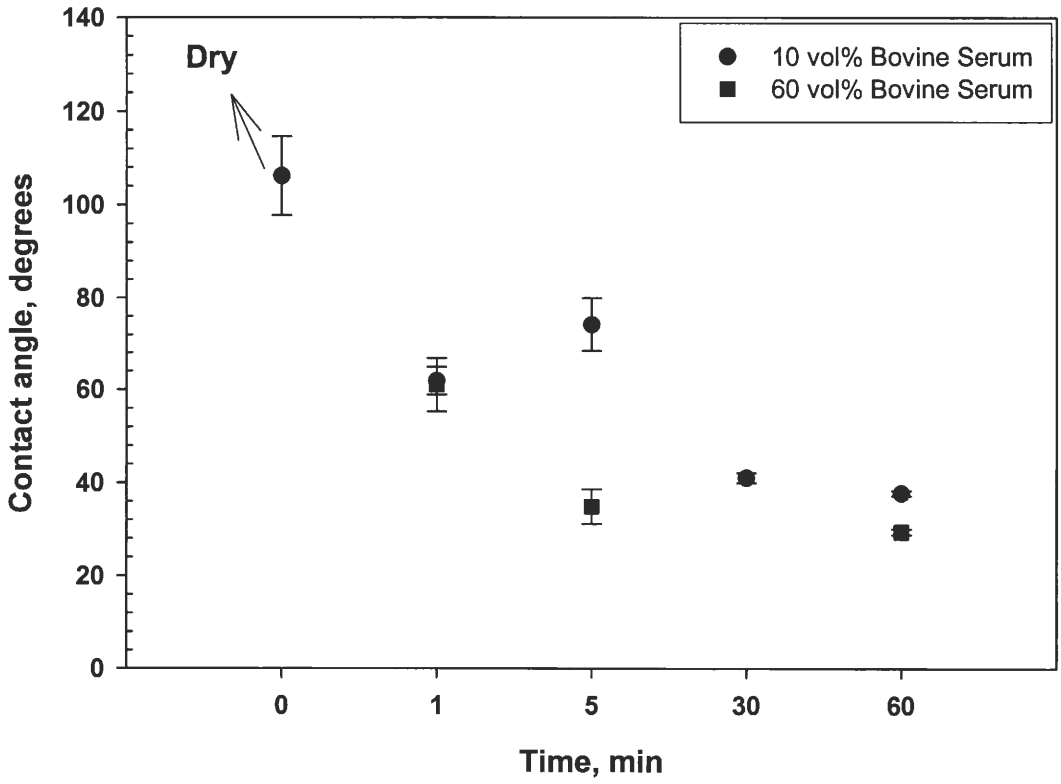

Figure 4.10 Contact angle measurements on UHMWPE as a function of soaking time in bovine serum at two different concentrations.

Figure 4.11 shows the pictures of droplets on dry, unsoaked UHMWPE and 60 vol% - 1 hour soaked sample. One can clearly observe the change in the hydrophobicity of the UHMWPE when proteins are introduced.

4.9 Discussion

The interfacial shear strengths measured on dry UHMWPE are slightly higher than those measured using macroscale torsion tests (1-7 MPa) [33]. Our data clearly shows that protein adsorption results in an increase in the interfacial shear strength of UHMWPE. The fact that the polymer exposed to higher concentration solution exhibits higher interfacial shear strength than the polymer exposed to the lower concentration solution supports the idea that shear strength appears to increase as the adsorbed protein content is increased. As the exposure time to protein solutions is increased, the interfacial shear strength increases in the

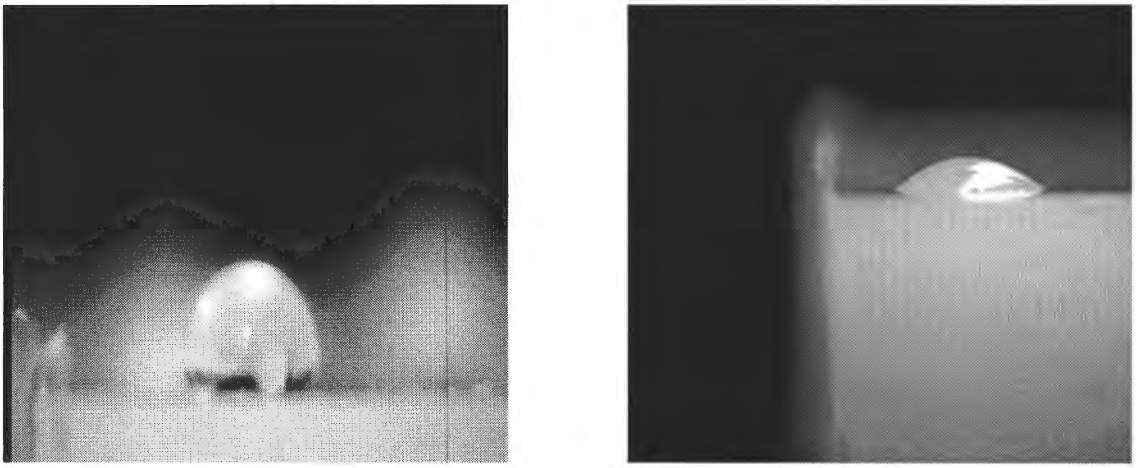

Figure 4.11 Droplet image on (a) unsoaked UHMWPE (b) UHMWPE soaked for 1 hour in 60 vol% BSA

case of a 60% protein solution but remains more or less comparable in the case of a 10% solution. This behavior is fairly consistent with the fluorescence data which suggests that the protein adsorption in the case of the 10% solution does not substantially increase with soaking time while that of the 60% solution shows a slight increase. The observed increase in interfacial shear strength due to protein adsorption also supports speculations made by researchers regarding the role of proteins on the interfacial shear strengths. Widmer et.al. [48] showed that hydrophobic polyethylene surfaces exhibit higher friction than hydrophilic ones and demonstrated that denatured proteins in solution adsorb preferentially onto hydrophobic surfaces rather than native proteins. They used Optical waveguide lightmode spectroscopy (OWLS) to show that proteins adsorbed onto hydrophobic surfaces occupy more surface area than those that adsorb onto hydrophilic surfaces. They therefore suggested that proteins denature during adsorption onto a hydrophobic surface. The denaturing of proteins upon adsorption on hydrophobic surfaces has been reported by other research groups [54] [55] as well. The results reported in this chapter provide good evidence that in our experiments, proteins denature upon adsorption onto dry hydrophobic UHMWPE. The proteins occupy large surface area, with hydrophobic parts undergoing adsorption, exposing hydrophilic regions. This adsorption mechanism is also evident from the contact angle measurements (Figure 4.10) where the protein-exposed samples show much lower contact angles compared to hydrophobic, dry UHMWPE sample. The data also shows that the samples with lower contact angle (and hence more denatured proteins) tend to exhibit higher interfacial shear strength. Thus, a denatured protein layer forms a high shear strength layer that is not conducive to boundary lubrication.

4.10 Conclusions

This study reports interfacial shear strengths for UHMWPE (a TJR biomaterial) as a function of exposure time to BSA of two different concentrations. The results show that concentration of the bovine serum and soaking time in bovine serum clearly affects the friction behavior of UHMWPE. At a low concentration of the bovine serum (10 vol%), the soaking time does not seem to have an effect on the frictional behavior of UHMWPE whereas at higher concentrations (60 vol%), the soaking time seems to affect the friction behavior significantly. This increase in frictional behavior of UHMWPE is also evident from our contact angle measurements where the protein-exposed samples show much lower contact angles compared to hydrophobic, dry UHMWPE sample. The increase in frictional behavior of UHMWPE when soaked in bovine serum is attributed to the formation of an adsorbed layer of denatured proteins on the surface. Such a protein layer is not conducive to boundary lubrication.

CHAPTER 5. Summary and future work

This thesis investigated methods to perform quantitative friction force microscopy and subsequently investigated the friction behavior of a biomaterial used in joint implants. The results from the studies are summarized below.

Comparison of lateral force calibration techniques:

In this study, we have analyzed and compared three lateral calibration methods (Ogletree et.al, Ruan and Bhushan, Cain et.al.) on a silicon sample. Cain et.al.'s method could not be used for the load range and the cantilever setup we used. Ogletree's method and Ruan and Bhushan's method were performed on silicon and lateral calibration factors were obtained. The values obtained differed by almost two orders of magnitude between the two methods, with Ruan and Bhushan's method yielding a lower value.

Quantification of interfacial shear stress of ultra high molecular weight polyethylene (UHMWPE):

These lateral calibration procedures were used to obtain quantitative friction data and interfacial shear stress on UHMWPE (biomaterial) sample. The shear strength value from Ruan and Bhushan's method were comparable to literature values. It was concluded that for the soft commercial Si_3N_4 cantilevers used Ruan and Bhushan's method yielded more appropriate reliable calibration factors, whereas Ogletree's and Cain's methods are more suitable for stiffer cantilevers.

In summary, quantitative friction force microscopy can be performed if the correct calibration method is utilized, careful calibration of the normal spring constant of the cantilever is performed and the probe radius/shape is determined and monitored throughout experiments.

The influence of protein adsorption on the friction behavior of UHMWPE:

The effect of soaking time in bovine serum and concentration of bovine serum on frictional behavior of UHMWPE samples were analyzed. The immersion of samples in bovine serum increased the friction and shear strength of the UHMWPE – Si_3N_4 interface. But, at a lower concentration (10 vol%) of bovine serum, the soaking time did not have an effect on the friction and shear strength. At a higher concentration (60 vol%), the friction and shear strength increased as the soaking time was increased. The friction data was well supported by contact angle and fluorescence measurements. The presence of denatured proteins on the hydrophobic polymeric surface was suggested as the reason for the increase in friction and a higher shear strength layer to be formed on the polymeric surface.

Recommendations and future Work

From literature, hydrophilic surfaces seem to have a different kind of protein adsorption than hydrophobic surfaces. Shear strengths of hydrophilic UHMWPE interface can be examined in future. Also, the synovial fluid consists of various components other than albumin proteins. The effect of each component on the friction and shear strength could be studied separately which will aid in the better design of biomaterials that are compatible with the component and which can minimize friction and wear. All these experiments should be

performed in the actual fluid to better simulate the original fluid environment of the human joints. This will also eliminate any capillary force affects. Some of the other future studies that could be pursued are: Effect of surface roughness on the adsorption of proteins on polymeric surfaces and characterization of friction and shear strength of cartilages using AFM.

APPENDIX. MATLAB code for fitting a parabola to tip shape and determination of tip radius

Program to read the DI image

```
function [im1a,im1b] = readimage(file)

%This Program loads a 256x256 scan The input to this program is the standard file generated by Nanoscope IV software. Note that this program reads the scaling factorsassigned by the software and converts all values back into (nm)

fid = fopen(file,'rt');
for ii =1:112
  fgets(fid);
end;
test=fgets(fid);
soft=str2num(test(18:26));
for ii=114:548
  fgets(fid);
end
test=fgets(fid);
hard=str2num(test(49:58));
fclose(fid);
```

```
fid = fopen(file,'r','n');

fseek(fid,40960,'bof');

im1 = fread(fid,[256,512],'bit16');

im1a = (hard*soft)*((im1(:,1:256)-min(min(im1(:,1:256)))))/65536;

%im1b = im1(:,257:512); Return
```

Program to locate the maximum points on x and y profile

```
function [p1,p2] = locate( xpts,ypts,imsize )
```

%Calls curve.m which in turn calls fitting.m This program takes the information about the tip across the x-axis and y-axis and finds the max pts along the top of the tip. Use readimage_scaled.m to load you image first. The varible xpts is a matrix of x values that cross the tip in the x dir. along with all of the y values. i.e. xpts=image[100:164,:], ypts=image[:,100:164]. The image size should be in microns. NOTA BENE: imsize1 must be modified if your scan was not 256x256

```
imsize1=imsize/256;

h=size(xpts);

g=size(ypts);

h1=(1:h(1))*imsize1;

h2=(1:h(2))*imsize1;

g2=(1:g(2))*imsize1;

g1=(1:g(1))*imsize1;
```

```
yfit=max(xpts');

xfit=max(ypts);

p1=figure;

subplot(2,1,1); plot(h2,xpts')

subplot(2,1,2); plot(g2,xfit)


p2=figure;

subplot(2,1,1); plot(g1,ypts)

subplot(2,1,2); plot(h1,yfit)


[X1,RES1,fig1,Rc] = curve(yfit,imsize1);

[X2,RES2,fig2,Rc2] = curve(xfit,imsize1);

return;
```

Program for fitting a parabola

```
function [X,RES,ydata,f] = fitting(x0,ydata)


%Input the name of your file in the load function. The first column of the data file should be
x (xnot) values. The second col. should be y values. The function then utilizes a nonlinear
least square fit to fit the function f.


for i=1:length(ydata)

        xdata(i)=i;
```

```
end
ydata=ydata;
%Standard equation for a parabola used to fit the probe
f = inline('x(1)*(xdata-x(2)).^2+x(3)','x','xdata');
[x,resnorm]=lsqcurvefit(f,x0,xdata(:),ydata(:));
x0=x;
[x,resnorm] = lsqcurvefit(f,x0,xdata,ydata);
%The unknown values along with the residual value are passed out of the function
X=x;
RES=resnorm;
```

Program for best fit by iterative routine

```
function [X,RES,fig,Rc,xmax] = curve(ydata,imsize)

%This program utilizes fitting.m to find the lowest residual value and the best fit. It then plots the laboratory data against the best fit line and gives values for the radius of curvature and curvature in (nm).

y=ydata;
%This is the initial guess for the three unknowns
x0=[1,.2,325];
%Iteratively calling fitting.m to find the best fit
[X,RES,y,f] = fitting(x0,y);
```

```
n=0;
while (RES)>=1e-6
   x0=X;
   [X,RES,y,f] = fitting(x0,y);
   n=n+1;
   if n==30
      break
   end
end
X;
RESIDUAL=RES;
%Post processing
X(2)=X(2)*imsize;

xmax=sqrt(abs((max(y)-X(3))/X(1)))+X(2);
xmax=xmax*imsize;

%calculate the radius of curvature
Rc=((1+(2*X(1)*xmax-2*X(1)*X(2))^2)^(3/2))/(2*X(1))

X(2)=X(2)/imsize;
%End post processing
for i=1:length(y)
```

```
xdata(i)=i;
end

%Plotting laboratory data against best fit line
fig=figure; hold
plot(xdata*imsize,f(X,xdata))
plot(xdata*imsize,y,'o')
xlabel('')
ylabel('Height Data (nm)')
legend('NL least sq','data',sprintf('Radius of Curv. = %1.5f',Rc))
title('Find Radius of Curvature ')

return;
```

REFERENCES

[1] Bhushan, B. Handbook of micro/nano tribology. 2nd ed ed. Boca Raton: CRC Press; 1999.

[2] Bowden, F.P., Tabor, D. The Friction and Lubrication of Solids. 1950.

[3] Bhushan, B. 1999. Principles and applications of tribology (John Wiley).

[4] Binnig, G., Quate, C.F., Gerber, C. Atomic Force Microscope. Physical Review Letters 1986;56:930-933.

[5] Wiesendanger, R. Scanning Probe Microscopy and Spectroscopy: Methods and Applications. New York: Cambridge University Press; 1994.

[6] Bonnell, D. Scanning Probe Microscopy and Spectroscopy: Theory, Techniques and Applications. 2 ed. New York: Wiley-VCH; 2001.

[7] Mate, C.M., McClelland, G.M., Erlandsson, R., Chiang, S. Atomic-scale friction of a tungsten tip on a graphite surface. Physical Review Letters 1987;59:1942-1945.

[8] Bhushan, B., Ruan, J.A. Atomic-Scale Friction Measurements Using Friction Force Microscopy .2. Application to Magnetic Media. Journal of Tribology-Transactions of the Asme 1994;116:389-396.

[9] Koinkar, V.N., Bhushan, B. Effect of scan size and surface roughness on microscale friction measurements. Journal of Applied Physics 1997;81:2472-2479.

[10] Sundararajan, S., Bhushan, B. Topography-induced contributions to friction forces measured using an atomic force/friction force microscope. Journal of Applied Physics 2000;88:4825-4831.

[11] Cleveland, J.P., Manne, S., Bocek, D., Hansma, P.K. A nondestructive method for determining the spring constant of cantilevers for scanning force microscopy. Review of Scientific Instruments 1993;64:403-405.

[12] Senden, T.J., Ducker, W.A. Experimental-Determination of Spring Constants in Atomic-Force Microscopy. Langmuir 1994;10:1003-1004.

[13] Sader, J.E. Parallel beam approximation for V-shaped atomic force microscope cantilevers. Review of Scientific Instruments 1995;66:4583-4587.

[14] Sader, J.E., Larson, I., Mulvaney, P., White, L.R. Method for the calibration of atomic force microscope cantilevers. Review of Scientific Instruments 1995;66:3789-3798.

[15] Torii, A., Sasaki, M., Hane, K., Okuma, S. A method for determining the spring constant of cantilevers for atomic force microscopy. Measurement Science & Technology 1996;7:179-184.

[16] Tortonese, M., Kirk, M. Characterization of application specific probes for SPMs. Proceedings of SPIE-The International Society for Optical Engineering 1997;3009:53-60.

[17] Sader, J.E., Chon, J.W.M., Mulvaney, P. Calibration of rectangular atomic force microscope cantilevers. Review of Scientific Instruments 1999;70:3967-3969.

[18] Holbery, J.D., Eden, V.L., Sarikaya, M., Fisher, R.M. Experimental determination of scanning probe microscope cantilever spring constants utilizing a nanoindentation apparatus. Review of Scientific Instruments 2000;71:3769-3776.

[19] Gibson, C.T., Weeks, B.L., Lee, J.R.I., Abell, C., Rayment, T. A nondestructive technique for determining the spring constant of atomic force microscope cantilevers. Review of Scientific Instruments 2001;72:2340-2343.

[20] Neumeister, J.M., Ducker, W.A. Lateral, Normal, and Longitudinal Spring Constants of Atomic-Force Microscopy Cantilevers. Review of Scientific Instruments 1994;65:2527-2531.

[21] Pietrement, O., Beaudoin, J.L., Troyon, M. A new calibration method of the lateral contact stiffness and lateral force using modulated lateral force microscopy. Tribology Letters 1999;7:213-220.

[22] Green, C.P., Lioe, H., Cleveland, J.P., Proksch, R., Mulvaney, P., Sader, J.E. Normal and torsional spring constants of atomic force microscope cantilevers. Review of Scientific Instruments 2004;75:1988-1996.

[23] Villarrubia, J.S. Algorithms for scanned probe microscope image simulation, surface reconstruction, and tip estimation. Journal of Research of the National Institute of Standards and Technology 1997;102:425-454.

[24] Villarrubia, J.S. Morphological Estimation of Tip Geometry for Scanned Probe Microscopy. Surface Science 1994;321:287-300.

[25] Khurshudov, A.G., Kato, K., Koide, H. Wear of the AFM diamond tip sliding against silicon. Wear 1997;203:22-27.

[26] Ruan, J.-A., Bhushan, B. Atomic-scale friction measurements using friction-force microscopy. Part I. General principles and new measurement techniques. Journal of Tribology 1994;116:378-388.

[27] Ogletree, D.F., Carpick, R.W., Salmeron, M. Calibration of frictional forces in atomic force microscopy. Review of Scientific Instruments 1996;67:3298-3306.

[28] Cain, R.G., Biggs, S., Page, N.W. Force calibration in lateral force microscopy. Journal of Colloid and Interface Science 2000;227:55-65.

[29] Liu, E., Blanpain, B., Celis, J.P. Calibration procedures for frictional measurements with a lateral force microscope. Wear 1996;192:141-150.

[30] Fujisawa, S., Kishi, E., Sugawara, Y., Morita, S. Lateral Force Curve for Atomic-Force Lateral Force Microscope Calibration. Applied Physics Letters 1995;66:526-528.

[31] Lantz, M.A., Oshea, S.J., Hoole, A.C.F., Welland, M.E. Lateral stiffness of the tip and tip-sample contact in frictional force microscopy. Applied Physics Letters 1997;70:970-972.

[32] Carpick, R.W., Ogletree, D.F., Salmeron, M. Lateral stiffness: A new nanomechanical measurement for the determination of shear strengths with friction force microscopy. Applied Physics Letters 1997;70:1548-1550.

[33] Park, K.D., Kim, J., Yang, S.J., Yao, A., Park, J.B. Preliminary study of interfacial shear strength between PMMA precoated UHMWPE acetabular cup and PMMA bone cement. Journal of biomedical materials research, Part B: Applied Biomaterials 2003;65B:272-279.

[34] Carpick, R.W., Agrait, N., Ogletree, D.F., Salmeron, M. Measurement of interfacial shear (friction) with an ultrahigh vacuum atomic force microscope. Journal of Vacuum Science & Technology B 1996;14:1289-1295.

[35] Major, R.C., Kim, H.I., Houston, J.E., Zhu, X.Y. Tribological properties of alkoxyl monolayers on oxide terminated silicon. Tribology Letters 2003;14:237-244.

[36] Pietrement, O., Troyon, M. Quantitative study of shear modulus and interfacial shear strength by combining modulated lateral force and magnetic force modulation microscopies. Surface and Interface Analysis 2001;31:1060-1067.

[37] Johnson, K.L., Kendall, K., Roberts, A.D. Surface Energy and Contact of Elastic Solids. Proceedings of the Royal Society of London Series a-Mathematical and Physical Sciences 1971;324:301-&.

[38] Enachescu, M., van den Oetelaar, R.J.A., Carpick, R.W., Ogletree, D.F., Flipse, C.F.J., Salmeron, M. Atomic force microscopy study of an ideally hard contact: The diamond(111) tungsten carbide interface. Physical Review Letters 1998;81:1877-1880.

[39] Bhushan, B. Modern Tribology Handbook. Boca Raton: CRC Press; 2001.

[40] Charnley, J. Anchorage of the Femoral Head Prosthesis to the Shaft of the Femur. Journal of Bone and Joint Surgery-British Volume 1960;42:28-30.

[41] Semlitsch, M., Willert, H.G. Clinical wear behaviour of ultra-high molecular weight polyethylene cups paired with metal and ceramic ball heads in comparison to metal-on-metal pairings of hip joint replacements. Proceedings of the Institution of Mechanical Engineers Part H-Journal of Engineering in Medicine 1997;211:73-88.

[42] Sauer, W.L., Anthony, M.E., 1998, Predicting the clinical wear performance of orthopaedic bearing surfaces, In: Jacobs, J.J., Graig, T. L. (Ed.) Alternative Bearing Surfaces in Total Joint Replacement, ASTM STP 1346. ASTM [American Society for Testing and Materials], pp. p. 1-29.

[43] Wang, A., Sun, D.C., Stark, C., Dumbleton, J.H. Wear Mechanisms of Uhmwpe in Total Joint Replacements. Wear 1995;181:241-249.

[44] Martin, D.F. Pathomechanics of Knee Osteoarthritis. Medicine and Science in Sports and Exercise 1994;26:1429-1434.

[45] Sawae, Y., Murakami, T., Chen, J. Effect of synovia constituents on friction and wear of ultra-high molecular weight polyethylene sliding against prosthetic joint materials. Wear 1998;216:213-219.

[46] Swann, D.A. Biochemistry of the vitreous. Bulletin de la Societe belge d'ophtalmologie 1987;223 Pt 1:59-72.

[47] Heuberger, M.P., Widmer, M.R., Zobeley, E., Glockshuber, R., Spencer, N.D. Protein-mediated boundary lubrication in arthroplasty. Biomaterials 2005;26:1165-1173. FIELD Reference Number: FIELD Journal Code:8100316 FIELD Call Number:.

[48] Widmer, M.R., Heuberger, M., Voros, J., Spencer, N.D. Influence of polymer surface chemistry on frictional properties under protein-lubrication conditions: implications for hip-implant design. Tribology Letters 2001;10:111-116.

[49] Park, S., Costa Kevin, D., Ateshian Gerard, A. Microscale frictional response of bovine articular cartilage from atomic force microscopy. Journal of biomechanics 2004;37:1679-1687.

[50] Ho, S.P., Carpick, R.W., Boland, T., LaBerge, M. Nanotribology of CoCr-UHMWPE TJR prosthesis using atomic force microscopy. Wear 2002;253:1145-1155.

[51] Van Straaten, J., Peppas, N.A. ATR-FTIR analysis of protein adsorption on polymeric surfaces. Journal of Biomaterials Science, Polymer Edition 1991;2:113-121.

[52] Xu, T., Fu, R., Yan, L. A new insight into the adsorption of bovine serum albumin onto porous polyethylene membrane by zeta potential measurements, FTIR analyses, and AFM observations. Journal of Colloid and Interface Science 2003;262:342-350.

[53] Balcells, M., Klee, D., Fabry, M., Hocker, H. Quantitative Assessment of Protein Adsorption by Combination of the Enzyme-Linked Immunosorbent Assay with Radioisotope-Based Studies. Journal of Colloid and Interface Science 1999;220:198-204.

[54] Norde, W., Giacomelli, C.E. BSA structural changes during homomolecular exchange between the adsorbed and the dissolved states. Journal of Biotechnology 2000;79:259-268.

[55] Ying, P., Yu, Y., Jin, G., Tao, Z. Competitive protein adsorption studied with atomic force microscopy and imaging ellipsometry. Colloids and Surfaces, B: Biointerfaces 2003;32:1-10.

ACKNOWLEDGMENTS

Firstly, I would like to thank my advisor, Dr. Sriram Sundararajan for his guidance and constant support throughout the course of my Master's research. I am looking forward with great enthusiasm and interest in working with him for my doctoral degree too. I would also like to extend my sincere thanks to my committee members Dr. Pranav Shrotriya and Dr. Balaji Narasimhan for agreeing to be on my thesis committee and also for their advice relating to research, whenever I needed.

My sincere appreciation to my research group colleagues Jason, Yilei, Satyam, Sharath, Vinay, Andrew and Jae-Joong for their willingness to discuss anything from research to politics. Andrew deserves a special mention for helping me during all my threatening encounters with MATLAB programming.

I would also like to thank Toshikazu Kawaguchi who helped me get access to Keck laboratory at ungodly hours and also his patience and enthusiasm in explaining concepts related to chemistry.

Thanks to Bob Doyle, Nikola Pekas, Salma Rahman, Amy Determan, Rajee Mani, Lakshminarasimhan and Jennifer Recknor for all their suggestions which helped me a great deal in my research.

I also thank Dr. Andrew Hillier for allowing me to use his laboratory for measurements.

Thanks to all my college buddies and friends in Ames for their constant encouragement.

Lastly, a special note of appreciation for my family for always being there whenever I needed them and without whom, I could not have reached here.